

Supporting Information

Self-Assembly of Russian Doll Concentric Porphyrin Nanorings

Sophie A. L. Rousseaux,[†] Juliane Q. Gong,[‡] Renée Haver,[†] Barbara Odell,[†] Tim D. W. Claridge,[†] Laura M. Herz[‡] and Harry L. Anderson^{†*}

[†] Department of Chemistry, University of Oxford, Chemistry Research Laboratory, Oxford, OX1 3TA, UK

[‡] Department of Physics, University of Oxford, Clarendon Laboratory, Oxford, OX1 3PU, UK

harry.anderson@chem.ox.ac.uk

Table of Contents

A. General Methods	S2
B. Synthetic Procedures	S3
<i>B1. Synthesis of Known Compounds</i>	<i>S3</i>
<i>B2. Synthesis of Novel Compounds</i>	<i>S3</i>
C. Assembly of the Russian Doll Structure and Control Mix	S7
<i>C1. Russian Doll Structure</i>	<i>S7</i>
<i>C2. Control Mix</i>	<i>S8</i>
<i>C3. Comparison of the ¹H NMR Spectra for the Russian Doll and the Control Mix</i>	<i>S10</i>
D. NMR Characterization of Novel Nanoring Structures	S11
<i>D1. Characterization of T6•c-P6•(Ar'CO₂)₆</i>	<i>S11</i>
<i>D2. Comparison of Δδ for T6 protons in T6•c-P6•(Ar'CO₂)₆ and T6•c-P6(Zn)</i>	<i>S16</i>
<i>D3. Characterization of T6•c-P6•(L1)₆•c-P12</i>	<i>S16</i>
<i>D4. Change in Chemical Shift for Protons in c-P12, T6•c-P6•(Ar'CO₂)₆ and Ligand L1 upon Formation of the Russian Doll Complex</i>	<i>S27</i>
E. Binding Studies	S28
<i>E1. Denaturation of c-P12•(Bn-L1)₆ with Quinuclidine</i>	<i>S28</i>
<i>E2. Denaturation of T6•c-P6•(L1)₆•c-P12 with Quinuclidine</i>	<i>S30</i>
<i>E3. Calculation of Effective Molarity</i>	<i>S31</i>
F. DOSY NMR Experiments	S32
<i>F1. Russian Doll</i>	<i>S32</i>
<i>F2. Control Mix</i>	<i>S33</i>
G. Photophysics	S34
<i>G1. Absorption Spectra</i>	<i>S34</i>
<i>G2. Fluorescence Spectra</i>	<i>S34</i>
<i>G3. Fluorescence Quantum Yields</i>	<i>S35</i>
<i>G4. Fluorescence Excitation Spectra</i>	<i>S35</i>
<i>G5. Measurement of Fluorescence Lifetimes</i>	<i>S36</i>
H. Russian Doll Templating	S37
<i>H1. Russian Doll Templated Synthesis of c-P12</i>	<i>S37</i>
<i>H2. Control Reaction</i>	<i>S38</i>
<i>H3. UV-Vis-NIR Spectra</i>	<i>S39</i>
<i>H4. Analytical GPC Traces</i>	<i>S40</i>
I. References	S41

A. General Methods

All reagents were purchased from commercial sources and solvents were used as supplied unless otherwise noted. Dry solvents (THF, CHCl₃, CH₂Cl₂ and toluene) were obtained by passing through alumina under N₂. Diisopropylamine was dried over calcium hydride, distilled and stored under N₂ over molecular sieves. NMR data were collected at 500 MHz using a Bruker AVII500 (with cryoprobe) or DRX500, or at 400 MHz using a Bruker AVII400 or AVIII400 at 298 K. Chemical shifts are quoted as parts per million (ppm) relative to residual CHCl₃ (at δ 7.27 ppm for ¹H NMR and at δ 77.2 ppm for ¹³C NMR) or CH₂Cl₂ (at δ 5.32 ppm for ¹H NMR and at δ 53.8 ppm for ¹³C NMR) and coupling constants (*J*) are reported in Hertz. DOSY experiments were carried out using the double stimulated echo sequence (DSTE),^{S1} which directly incorporates convection compensation. Diffusion coefficients were obtained by fitting intensity decays to $I = I_0 \exp(-D\gamma^2 \delta^2 g^2 (\Delta - \delta/3))$ where *I* and *I*₀ represent signal intensities in the presence and absence of gradient pulses respectively, *D* is the required diffusion coefficient, γ is the ¹H magnetogyric ratio, δ is the gradient pulse duration, Δ is the total diffusion time and *g* is the applied gradient strength (when corrected for sine-shaped gradient pulses). UV-vis-NIR absorbance measurements were recorded at 25 °C with a Perkin-Elmer Lambda 20 photospectrometer using quartz 1 cm cuvettes. UV-vis-NIR titrations were analyzed by calculating the difference in absorptions and plotted using OriginTM software. Size exclusion chromatography (SEC) was carried out using Bio-Beads S-X1, 200–400 mesh (Bio Rad). Analytical and semi-preparative GPC was carried out on Shimadzu Recycling GPC system equipped with LC-20 AD pump, SPD-M20A UV detector and a set of JAIGEL 3H (20 × 600 mm) and JAIGEL 4H (20 × 600 mm) columns in toluene as eluent with a flow rate of 3.5 mL/min.

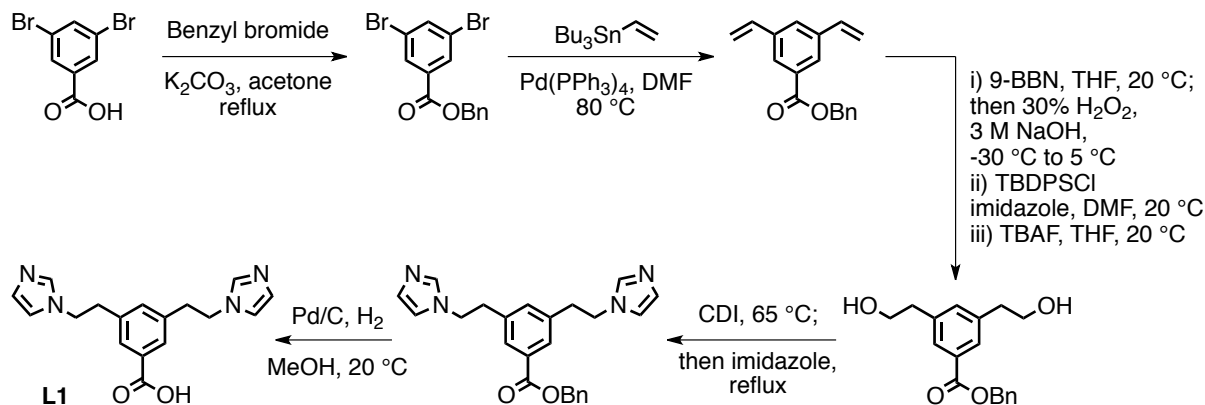
B. Synthetic Procedures

B1) Synthesis of Known Compounds

Porphyrin dimer **L-P2**,^{S2} porphyrin tetramer **L-P4**,^{S2} template **T6**,^{S3} nanoring **T6•c-P6(Zn)**^{S4} and nanoring **c-P12**^{S5} were prepared using previously reported procedures.

B2) Synthesis of Novel Compounds

Ligand L1



Benzyl 3,5-dibromobenzoate: To a solution of 3,5-dibromobenzoic acid (1.50 g, 5.36 mmol, 1.00 equiv) in acetone (27 mL, 0.20 M) was added K_2CO_3 (1.11 g, 8.04 mmol, 1.50 equiv) followed by benzyl bromide (0.64 mL, 5.41 mmol, 1.01 equiv). The resulting mixture was heated at reflux for 3 h. The solution was concentrated under reduced pressure and dissolved in EtOAc. The organic phase was washed with water ($\times 3$) and brine ($\times 1$), dried over Na_2SO_4 and concentrated under reduced pressure to afford 1.89 g (95% yield) of the desired product as a pale orange solid.

1H NMR (400 MHz, $CDCl_3$, 298 K): δ_H 8.13 (d, $J = 1.8$ Hz, 2H), 7.86 (t, $J = 1.8$ Hz, 1H), 7.46–7.36 (m, 5H), 5.37 (s, 2H). ^{13}C NMR (100 MHz, $CDCl_3$, 298 K): δ_C 163.9, 138.4, 135.3, 133.4, 131.4, 128.7, 128.6, 128.5, 123.0. MS (ESI): m/z 392.9 ($C_{14}H_{10}Br_2O_2$; $[M+Na]^+$ requires 392.9).

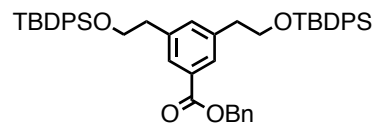
Benzyl 3,5-divinylbenzoate: The preparation of this compound was adapted from a literature procedure.^{S6} To a round-bottom flask containing benzyl 3,5-dibromobenzoate (1.88 g, 5.08 mmol, 1.00 equiv) and $Pd(PPh_3)_2Cl_2$ (358 mg, 0.508 mmol, 10.0 mol %) under argon was added dry DMF (40 mL, 0.13 M) and tributyl(vinyl)tin (3.56 mL, 12.2 mmol, 2.40 equiv). The solution was degassed by bubbling N_2 for 5 min, then stirred at $80\text{ }^\circ\text{C}$ for 2 h (by which time the reaction was judged to be complete by TLC). After cooling to room temperature, the reaction mixture was partitioned between ether and brine. The organic phase was stirred over an aqueous solution of 10% NaF (200 mL) for 3 h. The ether layer was separated, washed with water and brine, dried over Na_2SO_4 and concentrated under reduced pressure. Purification by column chromatography on silica gel (gradient of 1% to 4% Et_2O in PE 40–60) afforded 0.750 g (60% yield) of the desired compound as a clear oil.

1H NMR (400 MHz, $CDCl_3$, 298 K): δ_H 8.01 (d, $J = 1.2$ Hz, 2H), 7.62 (br s, 1H), 7.48–7.46 (m, 2H), 7.43–7.34 (m, 3H), 6.75 (dd, $J = 17.6, 10.9$ Hz, 2H), 5.84 (d, $J = 17.6$ Hz, 2H), 5.40 (s, 2H), 5.35 (d, $J = 10.9$ Hz, 2H). ^{13}C NMR (100 MHz, $CDCl_3$, 298 K): δ_C 166.3, 138.2, 136.0, 135.8,

130.8, 128.6, 128.3, 128.3, 126.7, 115.4, 66.9. **MS (ESI):** m/z 287.1 ($C_{13}H_{14}O_2$; $[M+Na]^+$ requires 287.1).

Benzyl 3,5-bis(2-((*tert*-butyldiphenylsilyl)oxy)ethyl)benzoate:

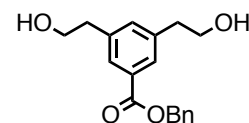
The preparation of this compound was adapted from literature procedures.^{S6,S7} To a solution of 9-BBN (0.5 M in THF, 29 mL, 14.7 mmol, 8.0 equiv) was added benzyl 3,5-divinylbenzoate (372 mg, 1.84 mmol, 1.00 equiv) as a solution in THF (9.0 mL, 0.20 M) and the resulting mixture was stirred at room temperature overnight (16 h). After cooling the reaction mixture to $-40\text{ }^\circ\text{C}$, H_2O_2 (30% in H_2O , 1.6 mL, 14.4 mmol, 8.0 equiv) was added slowly followed by 3.0 M NaOH (2.6 mL, 8.1 mmol, 4.4 equiv). The reaction mixture was then brought to $5\text{ }^\circ\text{C}$ and left to stir for 4 h at this temperature. At this point, the mixture was warmed to room temperature, neutralized by addition of 1 M HCl and finally concentrated under reduced pressure. Purification by column chromatography on silica gel (gradient of 80% EtOAc in PE 40–60 to 100% EtOAc) afforded 180 mg of a mixture of products containing the corresponding diol. This mixture was dissolved in dry DMF (3.0 mL, 0.2 M) and used without further purification.



The solution of impure diol in DMF was cooled to $0\text{ }^\circ\text{C}$ and placed under an atmosphere of nitrogen. Imidazole (245 mg, 3.60 mmol, 6.00 equiv) was added in one portion, followed by the dropwise addition of TBDPSCI (0.47 mL, 1.8 mmol, 3.0 equiv). The solution was allowed to warm to room temperature and stirred for 23 h (by which time the reaction was judged to be complete by TLC). The reaction mixture was diluted with H_2O and $Et_2O/EtOAc$ (1:1 mixture), the phases were separated and the aqueous phase was extracted with Et_2O ($\times 2$). The combined organic phases were washed with brine, dried over Na_2SO_4 and concentrated under reduced pressure. Purification by column chromatography on silica gel (gradient of 4% to 6% EtOAc in PE 40–60) afforded 282 mg (61% yield) of the desired compound as a clear oil.

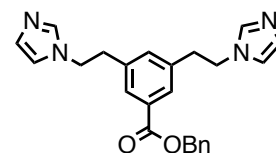
1H NMR (400 MHz, $CDCl_3$, 298 K): δ_H 7.73 (d, $J = 1.1$ Hz, 2H), 7.55 (d, $J = 6.6$ Hz, 8H), 7.44–7.29 (m, 17H), 7.14 (br s, 1H), 5.34 (s, 2H), 3.81 (t, $J = 6.8$ Hz, 4H), 2.82 (t, $J = 6.6$ Hz, 4H), 0.99 (s, 18 H). **^{13}C NMR (100 MHz, $CDCl_3$, 298 K):** δ_C 166.6, 139.4, 136.2, 135.5, 135.2, 133.7, 129.9, 129.5, 129.0, 128.5, 128.4, 128.2, 128.2, 128.1, 127.6, 66.5, 64.7, 38.9, 26.8, 19.1.

Benzyl 3,5-bis(2-hydroxyethyl)benzoate: To a solution of benzyl 3,5-bis(2-((*tert*-butyldiphenylsilyl)oxy)ethyl)benzoate (156 mg, 0.201 mmol, 1.00 equiv) in THF (4.0 mL, 0.05 M) was added TBAF (1.0 M in THF, 0.50 mL, 0.50 mmol, 2.5 equiv) dropwise. The reaction mixture was left to stir at room temperature overnight, then concentrated under reduced pressure. Purification by column chromatography on silica gel (gradient of 80% EtOAc in PE 40–60 to 100% EtOAc) afforded 51 mg (85% yield) of the desired compound as a clear oil.



1H NMR (400 MHz, $CDCl_3$, 298 K): δ_H 7.81 (d, $J = 1.1$ Hz, 2H), 7.46–7.34 (m, 5H), 7.32 (br s, 1H), 5.36 (s, 2H), 3.87 (t, $J = 6.5$ Hz, 4H), 2.89 (t, $J = 6.4$ Hz, 4H). **^{13}C NMR (100 MHz, $CDCl_3$, 298 K):** δ_C 166.6, 139.3, 135.9, 134.8, 130.4, 128.5, 128.2, 128.2, 66.7, 3.1, 38.7. **MS (ESI):** m/z 323.1 ($C_{18}H_{20}O_4$; $[M+Na]^+$ requires 323.1).

Benzyl 3,5-bis(2-(1*H*-imidazol-1-yl)ethyl)benzoate: The preparation of this compound was adapted from a literature procedure.^{S8} To a solution of benzyl 3,5-bis(2-hydroxyethyl)benzoate (47.0 mg, 0.156 mmol, 1.00 equiv) in toluene (0.80 mL, 0.20 M) was added CDI (58.0 mg, 0.360 mmol, 2.30 equiv). The mixture was stirred at $65\text{ }^\circ\text{C}$ for 10 min.

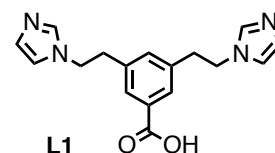


Imidazole (25.0 mg, 0.360 mmol, 2.30 equiv) was added next, the mixture was stirred at reflux for 60 h, and then concentrated under reduced pressure. Purification by column chromatography

on silica gel (gradient of 2% to 4% MeOH in DCM/1% Et₃N) afforded 35.0 mg (56% yield) of the desired product as a yellow oil.

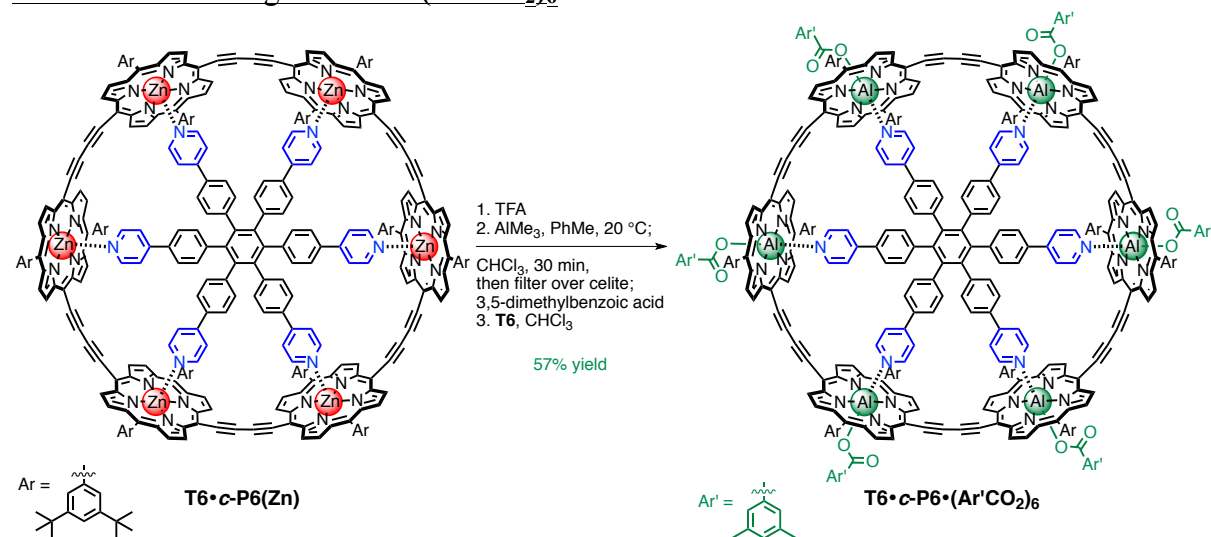
¹H NMR (400 MHz, CDCl₃, 298 K): δ_H 7.66 (d, *J* = 1.3 Hz, 2H), 7.56 (br s, 2H), 7.44–7.35 (m, 5H), 7.03 (br s, 2H), 6.86 (br s, 2H), 6.79 (br s, 1H), 5.32 (s, 2H), 4.18 (t, *J* = 6.9 Hz, 4H), 3.02 (t, *J* = 6.9 Hz, 4H). **¹³C NMR (100 MHz, CDCl₃, 298 K):** δ_C 165.8, 138.1, 136.9, 135.7, 133.8, 130.9, 128.6, 128.4, 128.3, 128.3, 128.2, 118.9, 66.9, 48.2, 37.1. **MS (ESI):** *m/z* 401.2 (C₂₄H₂₄N₄O₂; [M+H]⁺ requires 401.2).

Benzyl 3,5-bis(2-(1*H*-imidazol-1-yl)ethyl)benzoic acid: To Pd/C (10 wt %, 4.5 mg) under nitrogen was added benzyl 3,5-bis(2-(1*H*-imidazol-1-yl)ethyl)benzoate (17 mg, 0.043 mmol, 1.0 equiv) as a solution in MeOH (0.85 mL, 0.05 M). Under vigorous stirring, H₂ was bubbled through the solution for 15 min. At this point the reaction was stirred vigorously under an atmosphere of H₂ for 16 h (by which time the reaction was judged to be complete). The mixture was filtered over a short pad of celite using MeOH and concentrated under reduced pressure to afford 11 mg (83% yield) of the desired product as a pale yellow oil.

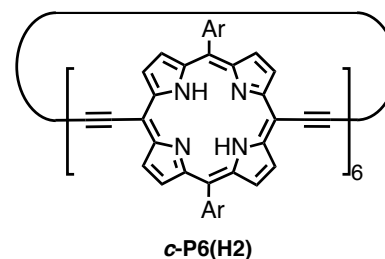


¹H NMR (500 MHz, CD₃OD, 298 K): δ_H 7.73 (br s, 2H), 7.65 (d, *J* = 1.0 Hz, 2H), 7.21 (br s, 2H), 7.08 (br s, 2H), 6.94 (br s, 1H), 4.29 (t, *J* = 7.0 Hz, 4H), 3.08 (t, *J* = 6.8 Hz, 4H). **¹³C NMR (125 MHz, CD₃OD, 298 K):** δ_C 171.5, 139.5, 138.3 (br), 135.5, 133.8, 129.4, 127.5 (br), 121.4 (br), 49.7, 37.9. **MS (ESI):** *m/z* 311.1 (C₁₇H₁₈N₄O₂; [M+H]⁺ requires 311.1).

Aluminum Nanoring T6•c-P6•(Ar'CO₂)₆



Free-base cyclic porphyrin hexamer c-P6(H₂): To a solution of T6•c-P6(Zn) (17.5 mg, 3.03 μmol, 1.00 equiv) in CHCl₃ (3.5 mL, 0.87 mM) at room temperature was added TFA (140 μL, 1.82 mmol, 600 equiv) dropwise. The reaction mixture was stirred at room temperature and the reaction progress was monitored by UV-vis spectroscopy. Upon completion (after 10 min), the reaction was quenched by the addition of pyridine (0.35 mL, 4.3 mmol, 1.4 × 10³ equiv)

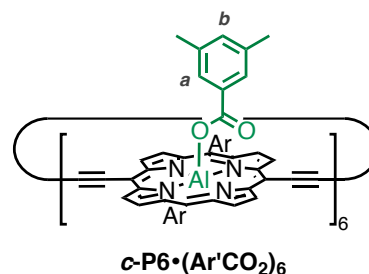


and *immediately* passed over a short plug of silica gel using CHCl₃/1% pyridine. The mixture was concentrated under reduced pressure to afford 12.4 mg (93% yield) of the desired product as a brown solid.

¹H NMR (400 MHz, CDCl₃, 298 K): δ_H 9.63 (d, *J* = 4.7 Hz, 24H, β-*H*), 8.82 (d, *J* = 4.7 Hz, 24H, β-*H*), 7.98 (d, *J* = 1.4 Hz, 24H, Ar-*H*_{ortho}), 7.81 (br t, *J* = 1.5 Hz, 12H, Ar-*H*_{para}), 1.52 (s, 216H, *t*-BuH). **¹³C NMR (125 MHz, CDCl₃, 298 K):** δ_C 149.8, 149.1, 139.8, 135.9, 132.5, 129.6, 124.4, 123.7, 121.4, 99.9, 93.3, 88.7, 35.0, 31.7. ***m/z* (MALDI-TOF)** 4401 (C₃₁₂H₃₁₂N₂₄, M⁺ requires 4398). **λ_{max} / nm (log ε)** 464 (5.46), 659 (5.00), 770 (5.20).

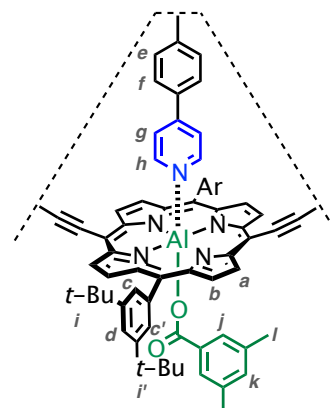
Aluminum cyclic porphyrin hexamer c-P6•(Ar'CO₂)₆:

To a solution of free-base **c-P6(H₂)** (12.4 mg, 2.82 μmol, 1.00 equiv) in dry toluene (0.56 mL, 5.0 mM) and under an atmosphere of argon was added AlMe₃ (2.0 M in hexanes, 9.3 μL, 19 μmol, 6.6 equiv) dropwise. The reaction mixture was left to stir at room temperature for 30 min, after which point the UV-vis-NIR spectrum indicated full conversion of the starting material. CHCl₃ was then added (approximately 3 mL). The mixture was stirred for 20–30 minutes until a precipitate formed, then filtered over celite into a flask containing 3,5-dimethylbenzoic acid (2.54 mg, 16.9 μmol, 6.00 equiv). After stirring at room temperature for 30 min, the ¹H NMR spectrum of the material indicated clean conversion to the desired product. This material was used without further purification.



¹H NMR (400 MHz, CDCl₃, 298 K): δ_H 9.78 (d, *J* = 4.7 Hz, 24H, β-*H*), 9.00 (d, *J* = 4.7 Hz, 24H, β-*H*), 7.85 (br s, 24H, Ar-*H*_{ortho}), 7.80 (br s, 12H, Ar-*H*_{para}), 6.13 (s, 6H, Ar-*H*_b), 4.88 (s, 12H, Ar-*H*_a), 1.51 (s, 36 H, CH₃), 1.49 (s, 216 H, *t*-BuH).

T6•c-P6•(Ar'CO₂)₆: To the sample of **c-P6•(Ar'CO₂)₆** in dry CHCl₃ (2.0 mL) was added hexapyridyl template **T6** (2.53 mg, 2.54 μmol). The solution was stirred at room temperature for 90 minutes, at which point the reaction appeared to be complete (monitored by UV-vis-NIR spectroscopy). The reaction mixture was purified by size exclusion chromatography on Biobeads SX-1 using CHCl₃ to yield 10.3 mg (57% yield from **c-P6(H₂)**) **T6•c-P6•(Ar'CO₂)₆** as a brown solid.



¹H NMR (400 MHz, CDCl₃, 298 K): δ_H 9.58 (d, *J* = 4.6 Hz, 24H, β-*H*_a), 8.87 (d, *J* = 4.6 Hz, 24H, β-*H*_b), 8.22 (br s, 12H, Ar-*H*_c or Ar-*H*_{c'}), 7.79 (br s, 12H, Ar-*H*_d), 7.29 (br s, 12H, Ar-*H*_c or Ar-*H*_{c'}), 6.31 (s, 6H, Ar-*H*_k), 5.52–5.47 (m, 24 H, Ar-*H*_e and Ar-*H*_f), 4.84 (d, *J* = 4.8 Hz, 12H, Ar-*H*_g), 4.50 (s, 12H, Ar-*H*_j), 1.68 (m, 12H, Ar-*H*_h), 1.64 (s, 36 H, Me-*H*_l), 1.62 (br s, 108 H, *t*-Bu-*H*_i or *t*-Bu-*H*_{i'}), 1.35 (br s, 108 H, *t*-Bu-*H*_i or *t*-Bu-*H*_{i'}).

¹H NMR (400 MHz, CD₂Cl₂, 298 K): δ_H 9.62 (d, *J* = 4.4 Hz, 24 H, β-*H*_a), 8.92 (d, *J* = 4.4 Hz, 24H, β-*H*_b), 8.33 (br s, 12H, Ar-*H*_c or Ar-*H*_{c'}), 7.86 (br s, 12H, Ar-*H*_d), 7.34 (br s, 12H, Ar-*H*_c or Ar-*H*_{c'}), 6.38 (s, 6H, Ar-*H*_k), 5.59 (d, *J* = 8.4 Hz, 12H, Ar-*H*_e), 5.52 (d, *J* = 8.4 Hz, 12H, Ar-*H*_f), 4.95 (br s, 12H, Ar-*H*_g), 4.47 (s, 12H, Ar-*H*_j), 1.69 (s, 36 H, Me-*H*_l), 1.63 (br s, 108 H, *t*-Bu-*H*_i or *t*-Bu-*H*_{i'}), 1.46 (m, 12H, Ar-*H*_h), 1.39 (br s, 108 H, *t*-Bu-*H*_i or *t*-Bu-*H*_{i'})

***m/z* (MALDI-TOF)** 5445 (C₄₃₈H₄₀₂Al₆N₃₀O₁₂, M⁺ – **T6** template requires 5443).

λ_{max} (CHCl₃) / nm (log ε) 483 (5.79), 752 (5.48), 784 (5.58), 820 (5.59).

C. Assembly of the Russian Doll Structure and Control Mix

C1) Russian Doll Structure

The Russian doll complex was prepared by ligand exchange of $\text{T6}\cdot\text{c-P6}\cdot(\text{Ar}'\text{CO}_2)_6$ with **L1** in the presence of **c-P12**. A solution of **c-P12** in CDCl_3 ($[\text{c-P12}] = 4.2 \times 10^{-4}$ M) was gradually added to an NMR tube containing a solution of $\text{T6}\cdot\text{c-P6}\cdot(\text{Ar}'\text{CO}_2)_6$ in CDCl_3 ($[\text{T6}\cdot\text{c-P6}\cdot(\text{Ar}'\text{CO}_2)_6] = 1.9 \times 10^{-4}$ M). Once a 1:1 ratio of the nanorings was reached, ligand **L1** was gradually added as a solution in CD_3OD ($[\text{L1}] = 0.16$ M) until the signals corresponding to the individual components disappeared and a new product appeared to have been formed (Figure S1). The crude mixture was purified by size exclusion chromatography on Biobeads SX-1 using CHCl_3 , concentrated under reduced pressure and dissolved in CD_2Cl_2 for further characterization (Figure S2 and Section D3). The Russian Doll complex is soluble in toluene- d_8 , CDCl_3 and CD_2Cl_2 however the sharpest NMR spectrum was obtained in CD_2Cl_2 .

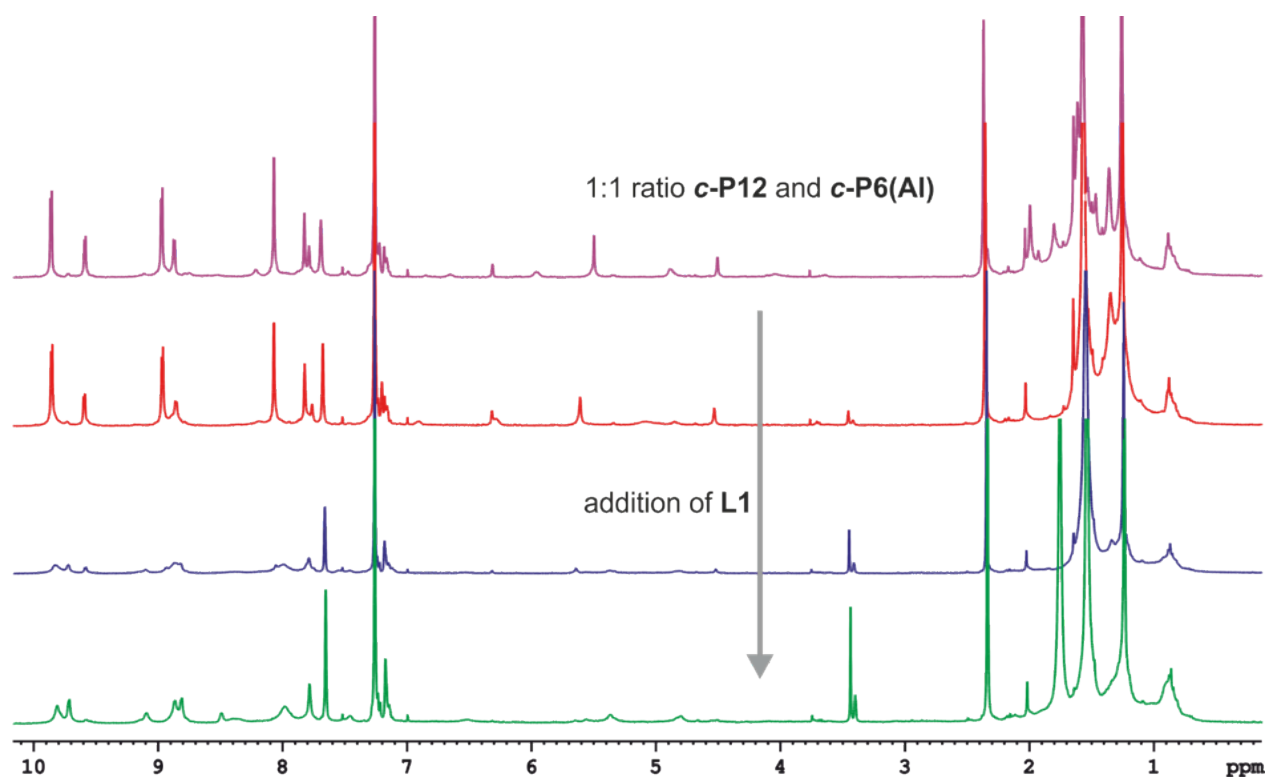


Figure S1. ^1H NMR titration of a 1:1 mixture of **c-P12** and $\text{T6}\cdot\text{c-P6}\cdot(\text{Ar}'\text{CO}_2)_6$ with **L1** (400 MHz, CD_2Cl_2 , 298 K). Ligand **L1** was added as a solution in CD_3OD ($[\text{L1}] = 0.16$ M).

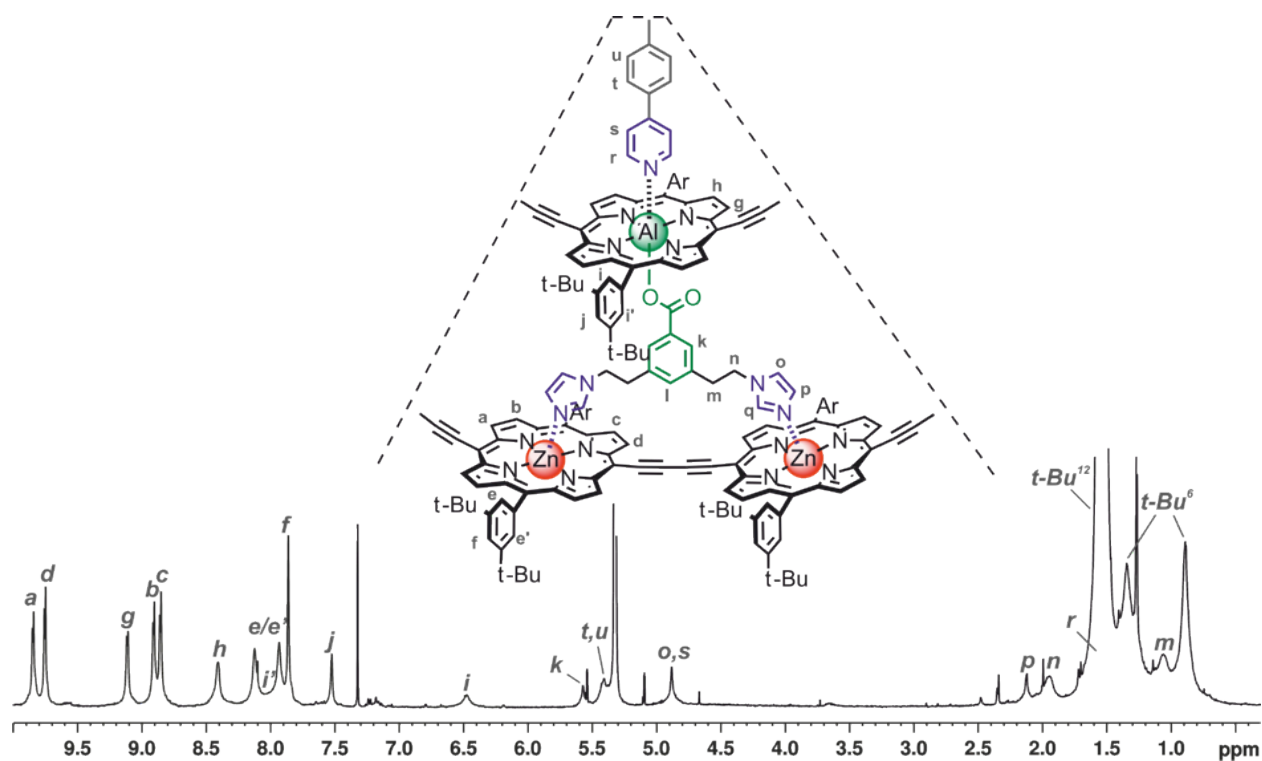


Figure S2. ^1H NMR spectrum of $\text{T6}\cdot\text{c-P6}\cdot(\text{L1})_6\cdot\text{c-P12}$ after purification by size exclusion chromatography on Biobeads SX-1 using CHCl_3 (400 MHz, CD_2Cl_2 , 298 K). See Section D3 for full characterization and peak assignments.

C2) Control Mix

The control mix was prepared in a similar fashion to the Russian doll structure. A solution of benzyl-protected ligand **Bn-L1** in CD_2Cl_2 ($[\text{Bn-L1}] = 4.8 \times 10^{-2} \text{ M}$) was gradually added to an NMR tube containing a solution of **c-P12** in CD_2Cl_2 ($[\text{c-P12}] = 1.7 \times 10^{-4} \text{ M}$). Once a 6:1 ratio of the protected ligand/nanoring was reached, a solution of $\text{T6}\cdot\text{c-P6}\cdot(\text{Ar}'\text{CO}_2)_6$ in CD_2Cl_2 ($[\text{T6}\cdot\text{c-P6}\cdot(\text{Ar}'\text{CO}_2)_6] = 5.7 \times 10^{-4} \text{ M}$) was gradually added until a 1:1 ratio of the nanorings was reached (Figure S3).

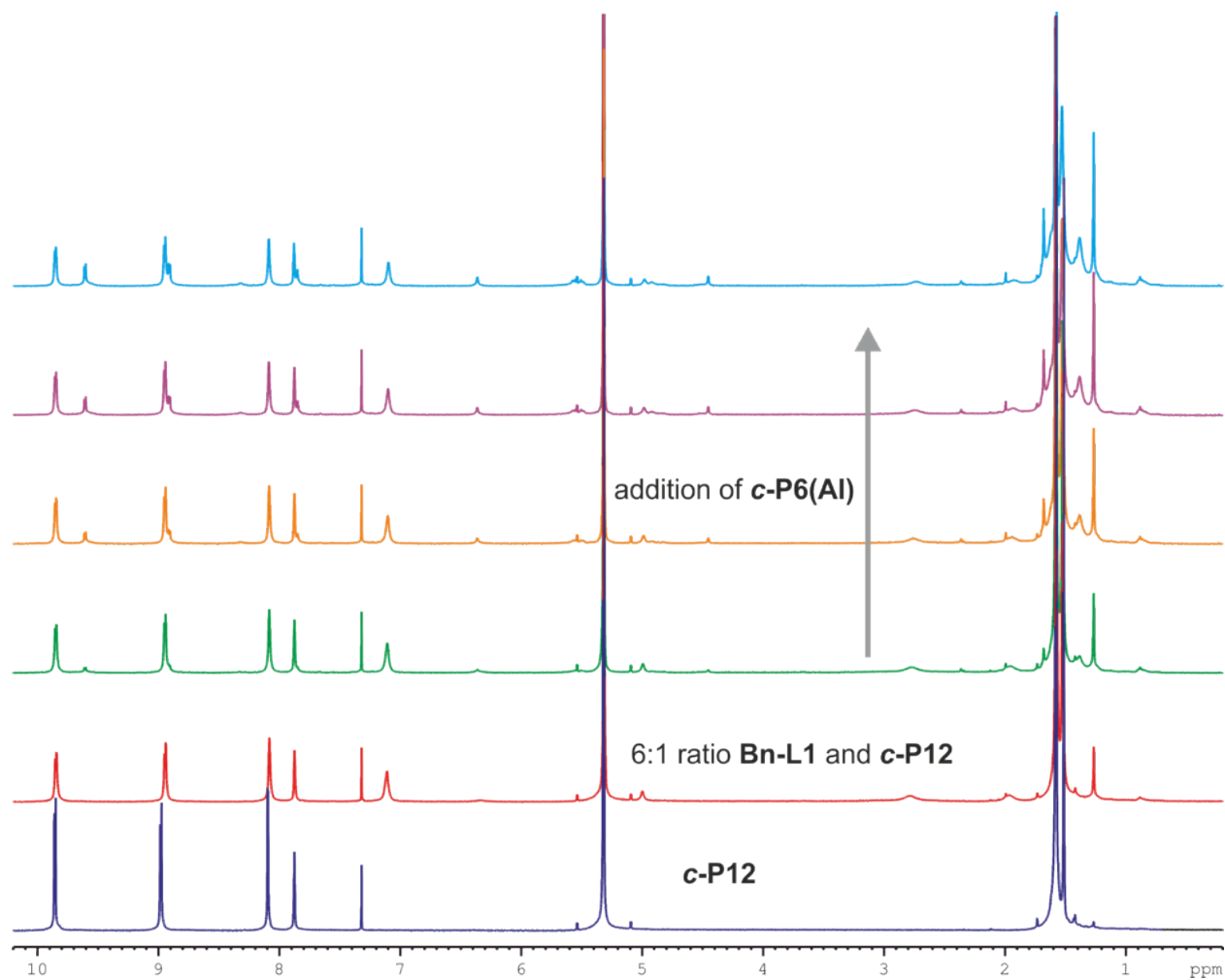


Figure S3. ¹H NMR titration of a 6:1 mixture of **Bn-L1** and **c-P12** with **T6•c-P6•(Ar'CO₂)₆** (400 MHz, CD₂Cl₂, 298 K).

C3) Comparison of the ^1H NMR Spectra for the Russian Doll and the Control Mix

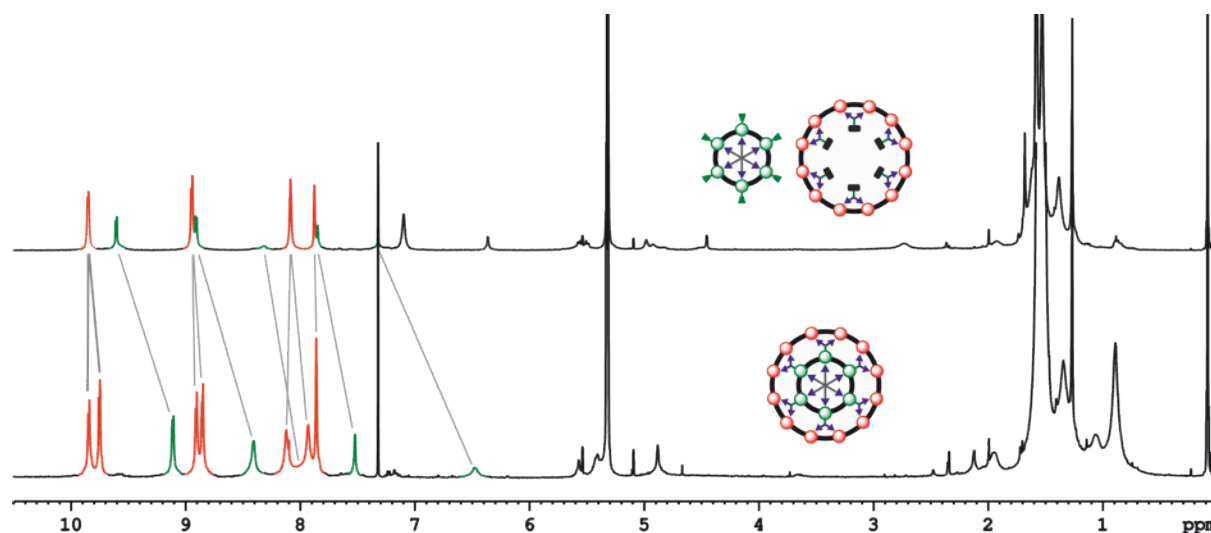


Figure S4. ^1H NMR spectra of the *control mix* (top spectrum) and the Russian doll complex (bottom spectrum) (400 MHz, CD_2Cl_2 , 298 K). The signals corresponding to the larger 12-porphyrin nanoring are highlighted in red while the signals corresponding to the aluminum 6-porphyrin nanoring are highlighted in green (see Section D for the full assignment of the ^1H NMR spectra of the various components). The protons from the inner Al-nanoring in the Russian doll are shielded compared to the free $\text{T6}\cdot\text{c-P6}\cdot(\text{Ar}'\text{CO}_2)_6$ in the control mixture, indicating that the smaller ring is nested within the larger ring.

The *control mix* (1.7×10^{-4} M in CD_2Cl_2) can be titrated with ligand **L1** ($[\text{L1}] = 0.16$ M in CD_3OD) to yield the Russian Doll complex (Figure S5). The signals are slightly broad at the titration endpoint but become sharper after removal of excess ligands by size exclusion chromatography in CHCl_3 .

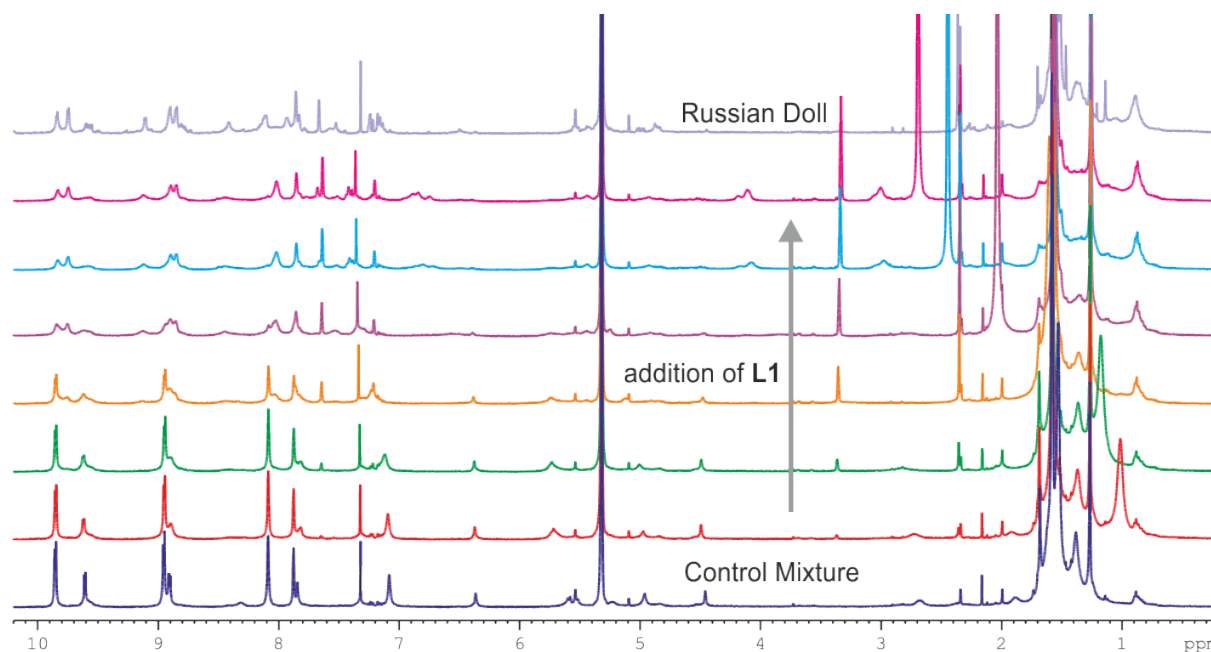


Figure S5. ^1H NMR titration of the *control mix* (1:1 ratio of $\text{c-P12}\cdot(\text{Bn-L1})_6$ and $\text{T6}\cdot\text{c-P6}\cdot(\text{Ar}'\text{CO}_2)_6$ with ligand **L1** (400 MHz, CD_2Cl_2 , 298 K). Ligand **L1** was added as a solution in CD_3OD ($[\text{L1}] = 0.16$ M in CD_3OD).

D. NMR Characterization of Novel Nanoring Structures

D1) Characterization of $T6 \cdot c-P6 \cdot (Ar'CO_2)_6$

Due to the high degree of symmetry in the aluminum 6-ring, only a “slice” corresponding to one sixth of the structure needs to be considered for the interpretation of the 1H NMR spectrum (Figure S6). The portion of the aryl side-group drawn in bold points towards template **T6**. The assignment of the 1H NMR spectrum is presented in the following section and was carried out using COSY, NOESY and HSQC NMR experiments. The similar zinc porphyrin system $T6 \cdot c-P6(Zn)$ was also used as a reference.^{S3}

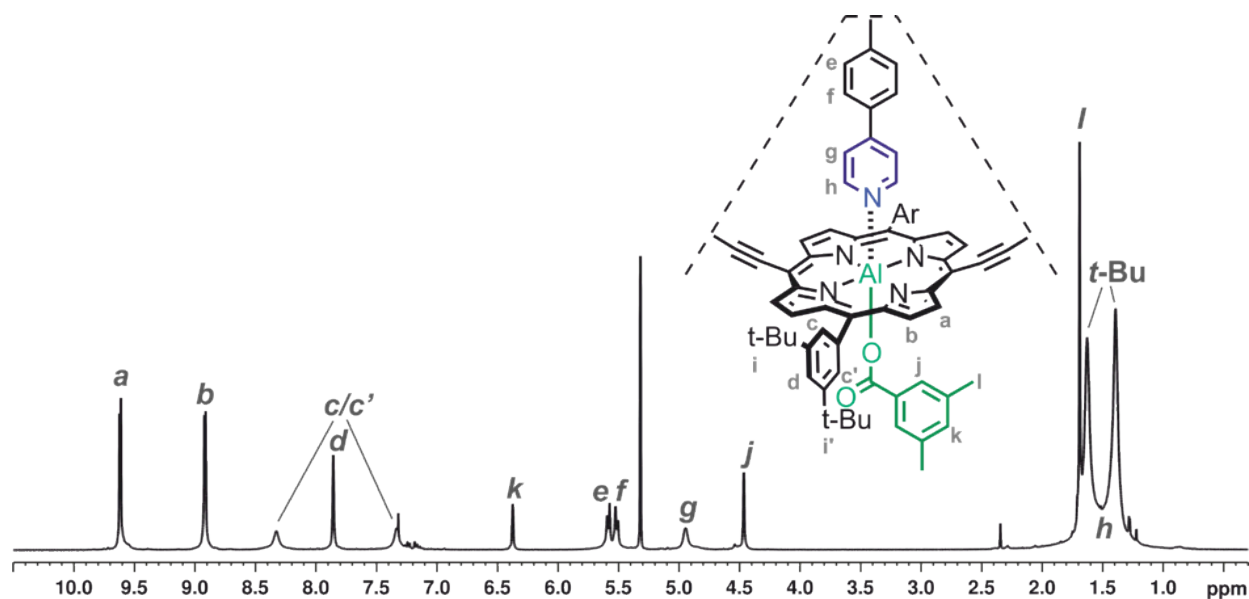


Figure S6. 1H NMR spectrum of $T6 \cdot c-P6 \cdot (Ar'CO_2)_6$ (400 MHz, CD_2Cl_2 , 298 K).

Our assignment of the 1H NMR spectrum begins with the β -protons **a** and **b** (Figure S7). Proton **a**, which is adjacent to the butadiyne bridge, is at the highest chemical shift (9.62 ppm). Proton **a** shows a NOE to proton **b**. Proton **b** also shows NOEs to protons **c** and **c'** (broad signals at 8.33 and 7.34 ppm).

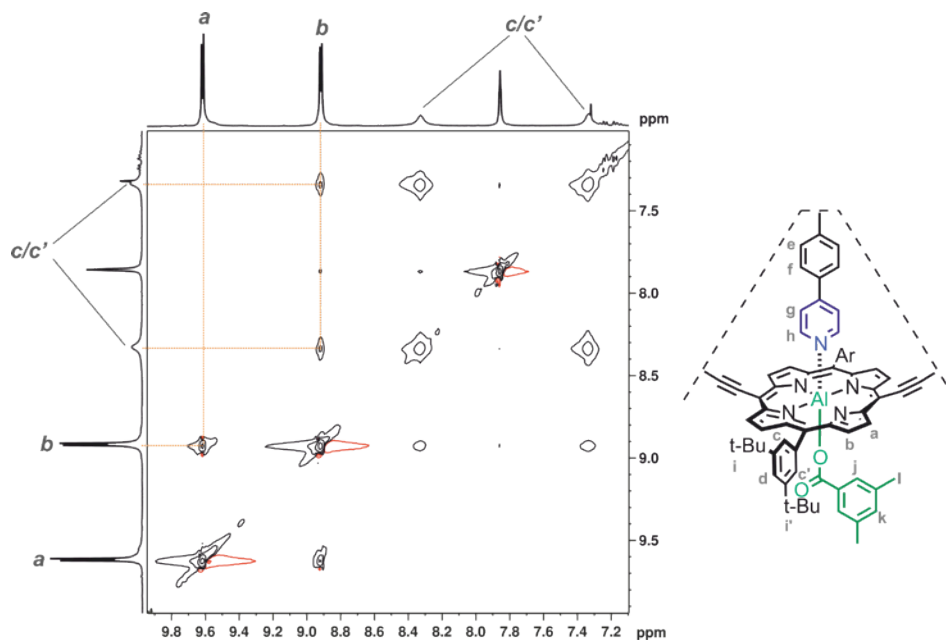


Figure S7. Region of the NOESY spectrum of **T6•c-P6•(Ar'CO₂)₆** corresponding to protons **a**, **b**, **c** and **c'** (400 MHz, CD₂Cl₂, 298 K, 600 ms mixing time).

NOEs are also observed between the *tert*-butyl group protons and protons **b**, **c** and **c'** (Figures S8). Strong NOEs are also observed between the *tert*-butyl group protons and the *para* proton **d** on the aryl side-group. This suggests that the aryl side-groups are rotating quickly on the T_1 timescale.

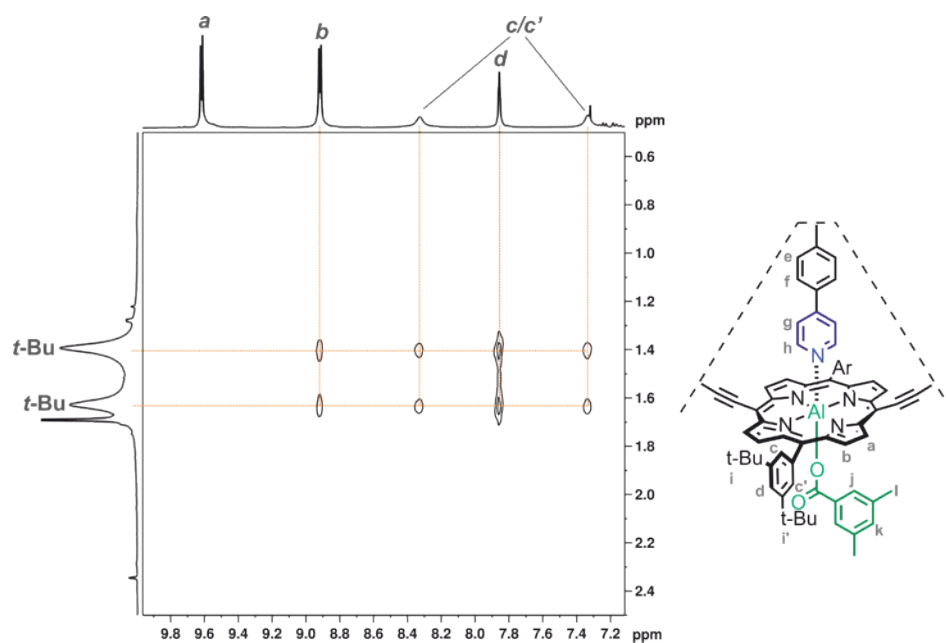


Figure S8. Region of the NOESY spectrum of **T6•c-P6•(Ar'CO₂)₆** corresponding to the *tert*-butyl protons on the aryl side-group and protons **b**, **c**, **c'** and **d** (400 MHz, CD₂Cl₂, 298 K, 600 ms mixing time).

In the COSY spectrum, correlations are observed between the CH_3 (protons *l*) group of the carboxylic acid ligand and protons *j* and *k* (Figure S9). Protons *j* and *k* are shielded due to ring current effects.

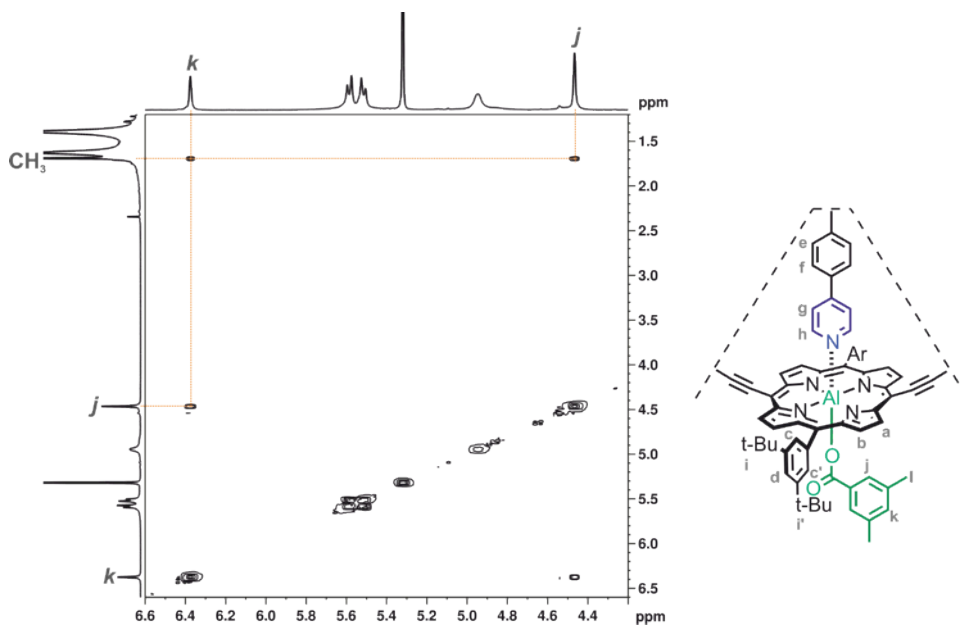


Figure S9. Region of the COSY spectrum of $\text{T6}\cdot\text{c-P6}\cdot(\text{Ar}'\text{CO}_2)_6$ corresponding to the protons on the carboxylic acid ligand (400 MHz, CD_2Cl_2 , 298 K).

The HSQC spectrum also confirms our assignments for the CH_3 and *t*-Bu protons, since these protons correlate with signals at 20.3 and 31.4 ppm, respectively (Figure S10).

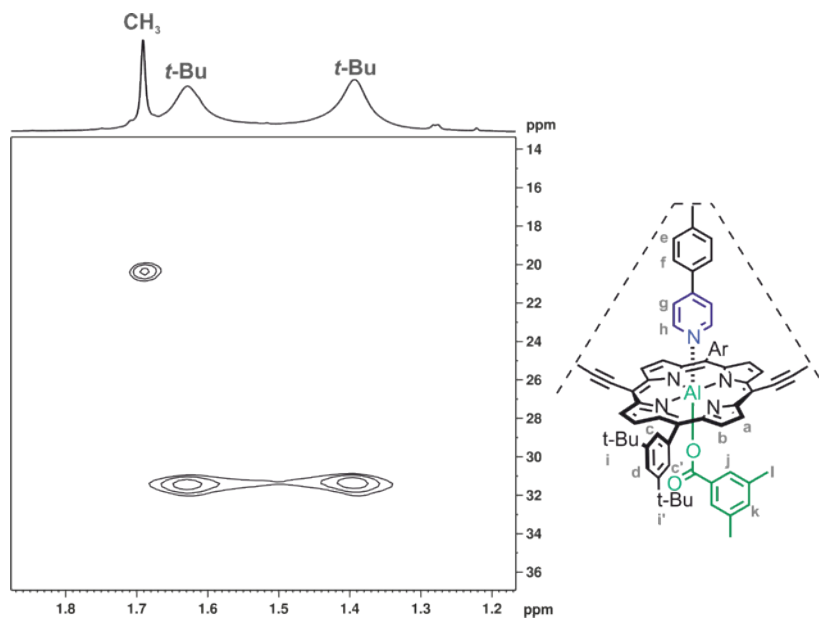


Figure S10. Region of the HSQC spectrum of $\text{T6}\cdot\text{c-P6}\cdot(\text{Ar}'\text{CO}_2)_6$ corresponding to the CH_3 and *t*-Bu protons (400 MHz, CD_2Cl_2 , 298 K).

The HSQC spectrum also supports our assignments for the aromatic protons in **T6•c-P6•(Ar'CO₂)₆** (Figure S11). Protons *a* and *b* correlate with signals at 130.3 and 133.4 ppm, respectively. Protons *c* and *c'* correlate with signals at 128.7 and 129.6 ppm, respectively, while proton *d* correlates with a signal at 121.7 ppm. Protons *j* and *k* from the carboxylic acid ligand correlate with signals at 124.9 and 130.8 ppm, respectively.

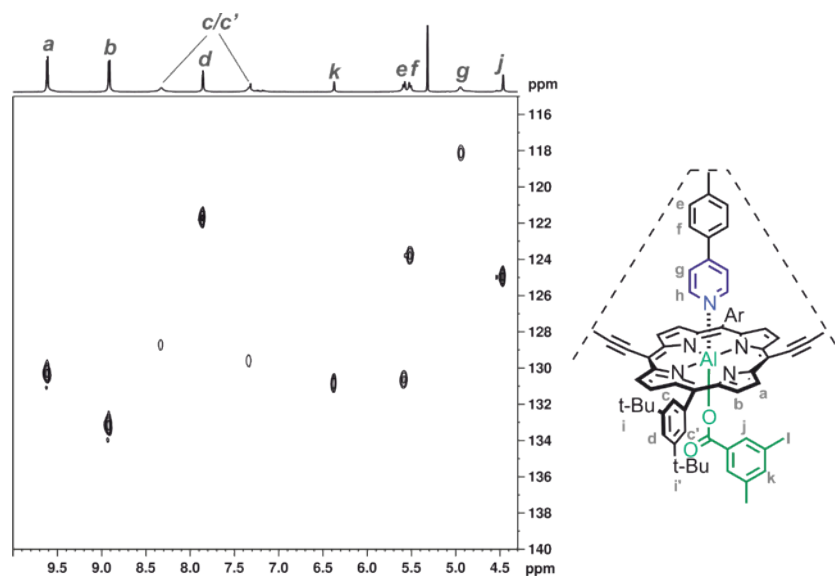


Figure S11. Region of the HSQC spectrum of **T6•c-P6•(Ar'CO₂)₆** corresponding to protons *a*, *b*, *c*, *c'*, *d*, *e*, *f*, *g*, *j* and *k* (400 MHz, CD₂Cl₂, 298 K).

Due to ring current effects, the α -pyridyl proton *h* on template **T6** is shielded and appears at low chemical shift. The HSQC spectrum helped to assign proton *h* at 1.46 ppm due to its correlation with the signal at 141.5 ppm, which is characteristic of the α -carbon in a pyridine ring (Figure S12).

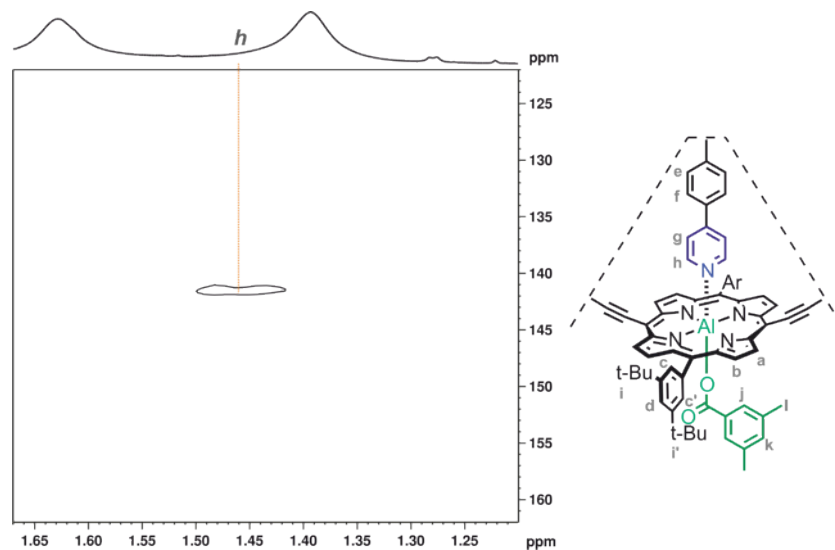


Figure S12. Region of the HSQC spectrum of **T6•c-P6•(Ar'CO₂)₆** corresponding to template proton *h* (400 MHz, CD₂Cl₂, 298 K).

Template protons *e* and *f* were assigned based on their correlation in the COSY spectrum (Figure S13) and the relative strength of their NOEs with proton *g* in the NOESY spectrum (Figure S14).

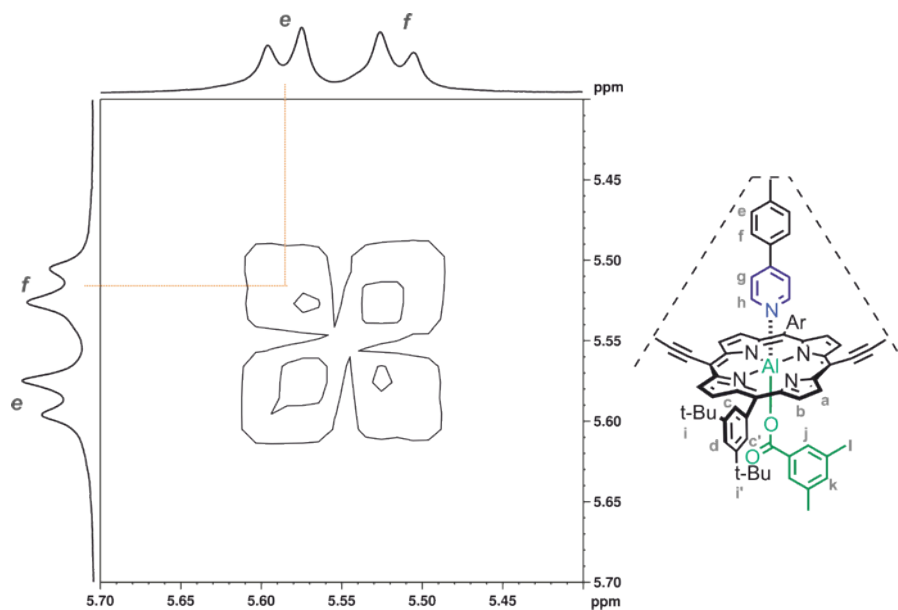


Figure S13. Region of the COSY spectrum of $\text{T6}\cdot\text{c-P6}\cdot(\text{Ar}'\text{CO}_2)_6$ corresponding to template protons *e* and *f* (400 MHz, CD_2Cl_2 , 298 K).

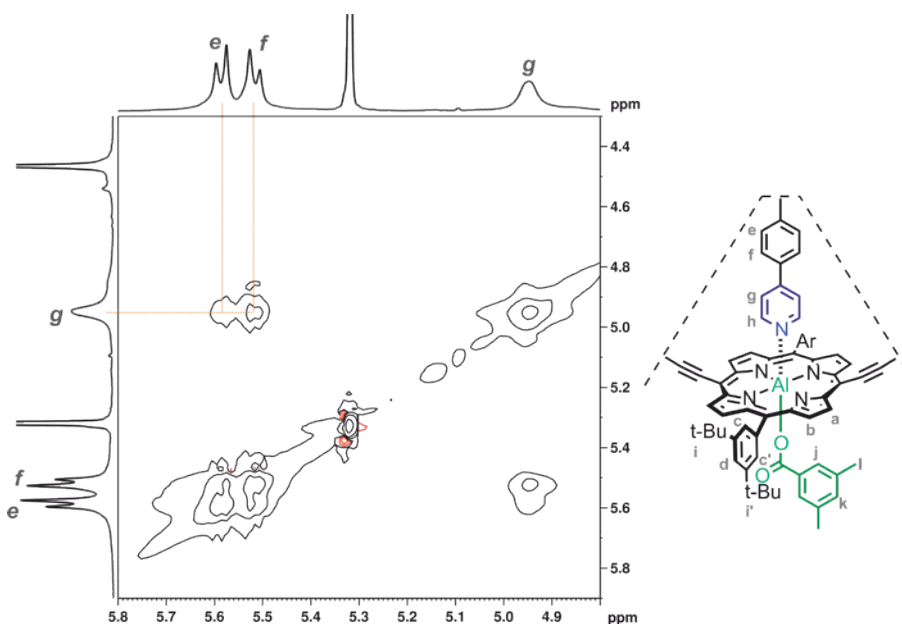


Figure S14. Region of the NOESY spectrum of $\text{T6}\cdot\text{c-P6}\cdot(\text{Ar}'\text{CO}_2)_6$ corresponding to template protons *e*, *f* and *g* (400 MHz, CD_2Cl_2 , 298 K, 600 ms mixing time).

Finally, the assignments for protons *e*, *f* and *g* were confirmed based on their correlations with signals at 130.6, 123.7 and 118.2 ppm, respectively, in the HSQC spectrum (Figure S11).

D2) Comparison of $\Delta\delta$ for T6 protons in $\text{T6}\cdot\text{c-P6}\cdot(\text{Ar}'\text{CO}_2)_6$ and $\text{T6}\cdot\text{c-P6}(\text{Zn})$

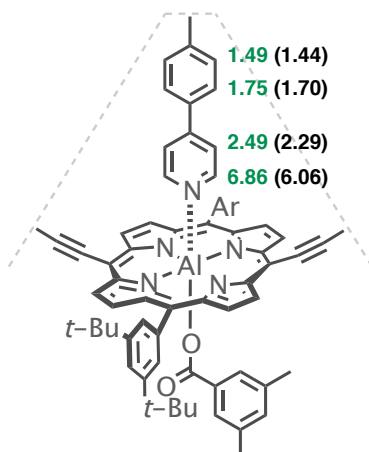


Figure S15. Complexation-induced changes in the chemical shift ($\Delta\delta$) in the ^1H NMR of free template **T6** and bound template **T6** (CDCl_3 , 298K) in $\text{T6}\cdot\text{c-P6}\cdot(\text{Ar}'\text{CO}_2)_6$ (green) and the reference $\text{T6}\cdot\text{c-P6}(\text{Zn})$ complex (black). The $\Delta\delta$ was calculated from $\delta_{\text{free}} - \delta_{\text{bound}}$.

The change in chemical shift ($\Delta\delta$) for template **T6** protons upon binding the 6-porphyrin nanoring can be calculated by subtracting the chemical shift of the proton in the complex (δ_{bound}) from the chemical shift of the proton in free **T6** (δ_{free}). These have been previously calculated for $\text{T6}\cdot\text{c-P6}(\text{Zn})$ and are indicated by the black numbers in parentheses in Figure S15.^{S3} The change in chemical shift upon complexation of **T6** in $\text{c-P6}\cdot(\text{Ar}'\text{CO}_2)_6$ (green numbers in Figure S15) are very similar to those observed for $\text{T6}\cdot\text{c-P6}(\text{Zn})$.

In the case of the aluminum 6-ring, the $\Delta\delta$ s are slightly larger, suggesting that the hexapyridyl template is closer to the plane of the porphyrin. The Al-N and Zn-N distances in related metalloporphyrin crystal structures (where N corresponds to the nitrogen in a pyridyl group) are very similar (2.215 and 2.15 Å, respectively).^{S4,S9} In hexacoordinate Al-porphyrins, the metal is in the plane of the porphyrin.^{S9,S10} However, in $\text{T6}\cdot\text{c-P6}(\text{Zn})$, the mean distance between the porphyrin plane and the Zn atom is 0.24 ± 0.06 Å, thus pushing the template further from the plane of the porphyrin and decreasing the observed $\Delta\delta$.^{S4}

D3) Characterization of $\text{T6}\cdot\text{c-P6}\cdot(\text{L1})_6\cdot\text{c-P12}$

Due to the high degree of symmetry in the Russian doll complex, only a “slice” corresponding to one sixth of the structure needs to be considered for the interpretation of the ^1H NMR spectrum (Figure S16). The chemical structure of this “slice” contains one aluminum porphyrin and two zinc porphyrins as well as one equivalent of the bridging ligand **L1** and one “leg” of the hexapyridyl template **T6**. For the aluminum 6-ring, the portion of the aryl side-group drawn in bold points towards template **T6** while the rest of the aryl side-group points toward the bridging ligand and the larger 12-porphyrin ring. For the zinc 12-ring, the part of the aryl side-group drawn in bold points towards the inside of the Russian doll (i.e. towards the aluminum 6-ring). The nearly complete assignment of the ^1H NMR spectrum for the Russian doll complex is detailed in the following section. These assignments are based on COSY, ROESY, NOESY and HSQC NMR experiments, as well as by comparison with similar porphyrin systems and the assignments obtained for $\text{T6}\cdot\text{c-P6}\cdot(\text{Ar}'\text{CO}_2)_6$ in the previous section. Protons **l** and **q** could not be unambiguously identified.

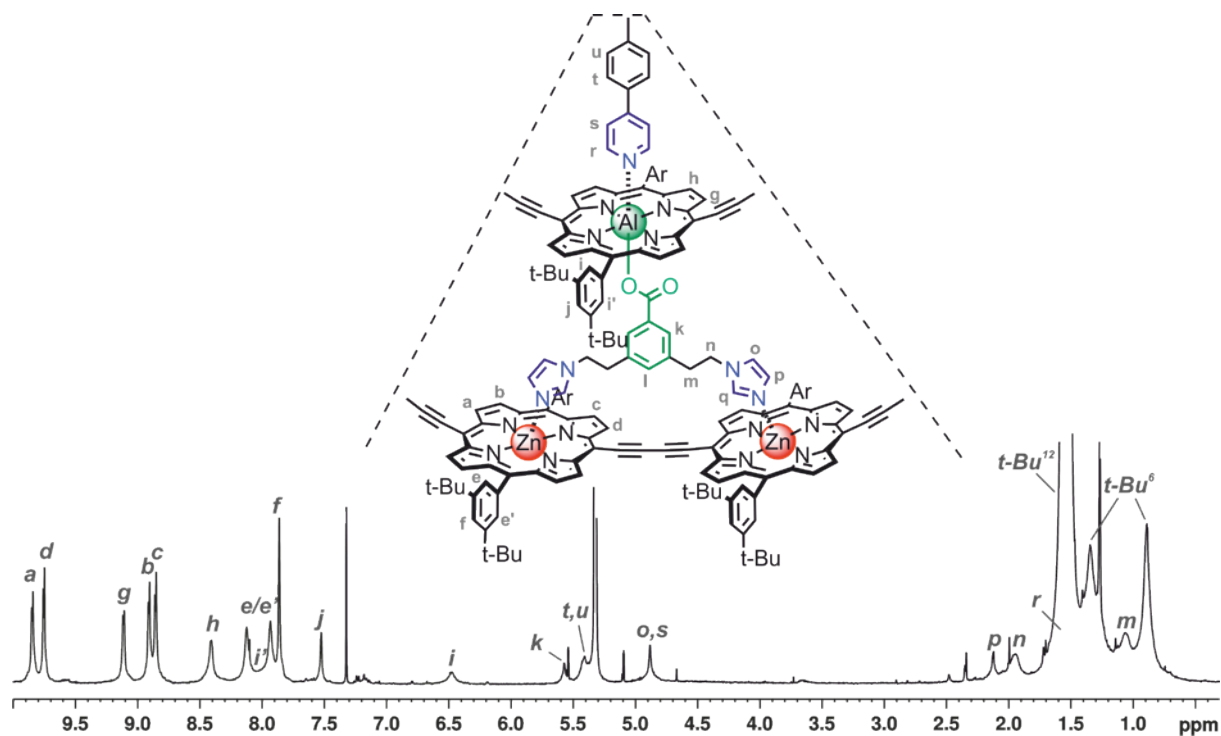


Figure S16. ^1H NMR spectrum of $\text{T6}\cdot\text{c-P6}\cdot(\text{L1})_6\cdot\text{c-P12}$ (400 MHz, CD_2Cl_2 , 298 K).

Our assignment of the ^1H NMR spectrum of the Russian doll complex begins with the β -protons from **c-P12**. Protons *a* and *d*, which are adjacent to the butadiyne, are at a higher chemical shift than protons *b* and *c*. Proton *a* was distinguished from *d* based on its NOE with ligand proton *p* (see Figure S29). Proton *a* shows a NOE with proton *b* while proton *d* shows a NOE with proton *c* (Figure S17). Coupling between *a/b* and *c/d* was also observed in the COSY spectrum.

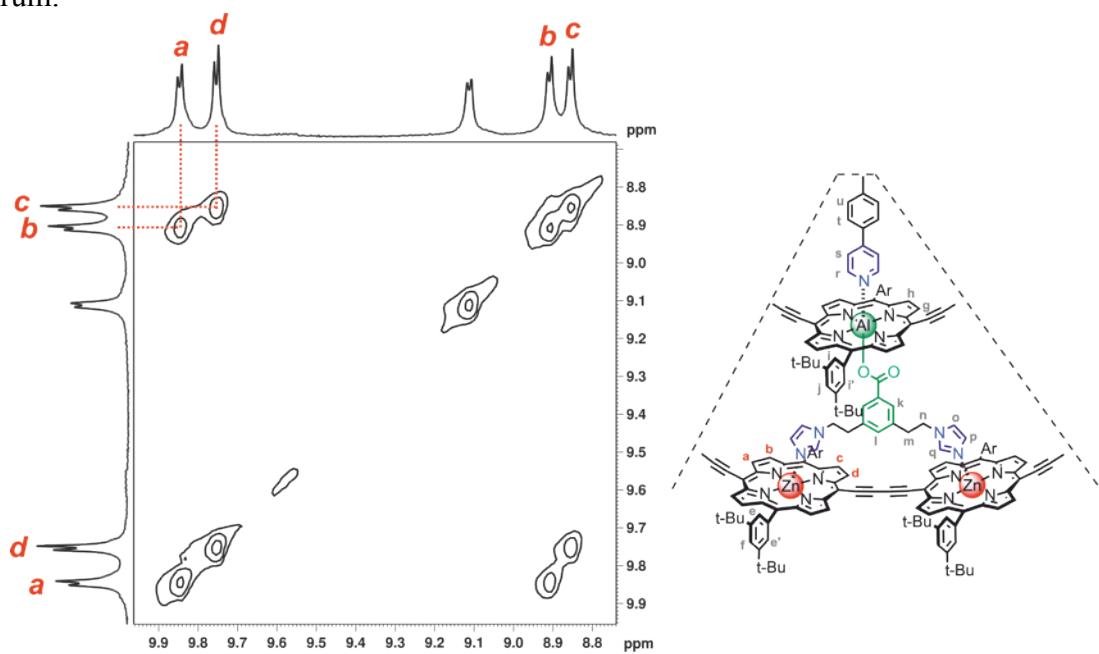


Figure S17. Region of the NOESY spectrum of $\text{T6}\cdot\text{c-P6}\cdot(\text{L1})_6\cdot\text{c-P12}$ corresponding to the β -protons in **c-P12** (400 MHz, CD_2Cl_2 , 298 K, 300 ms mixing time).

In the HSQC spectrum, protons *a* and *d* correlate with signals at 130.1 and 129.9 ppm, respectively (Figure S18). The third proton that correlates with a signal at 129.9 ppm must be proton *g* from *c*-P6. Similarly, protons *b*, *c* and *h* all correlate with signals of similar chemical shift (132.9, 132.9 and 132.8 ppm, respectively).

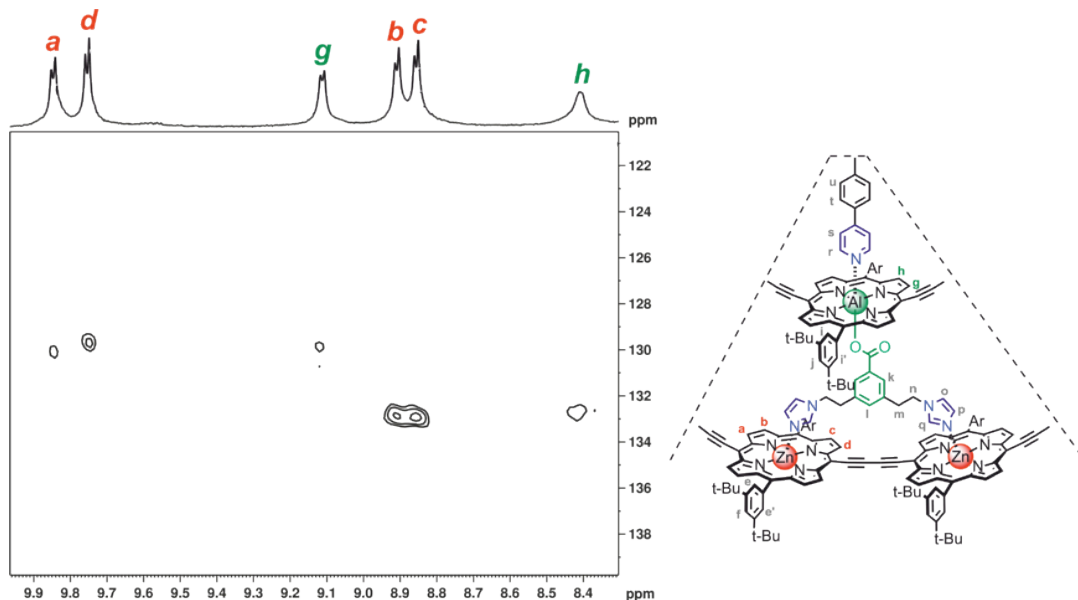


Figure S18. Region of the HSQC spectrum of **T6•c-P6•(L1)₆•c-P12** corresponding to the β-protons in *c*-P12 and *c*-P6 (400 MHz, CD₂Cl₂, 298 K).

The assignment of β-protons *g* and *h* from *c*-P6 is further confirmed by the presence of a NOE between these two signals (Figure S19). Coupling between *g* and *h* was also observed in the COSY spectrum.

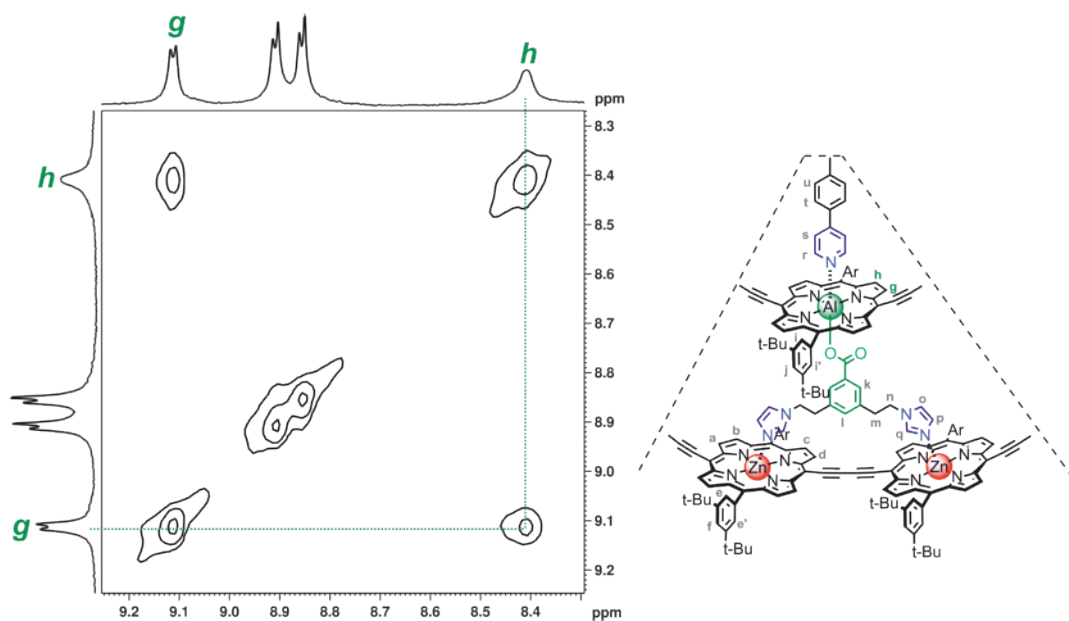


Figure S19. Region of the NOESY spectrum of **T6•c-P6•(L1)₆•c-P12** corresponding to the β-protons in *c*-P6 (400 MHz, CD₂Cl₂, 298 K, 300 ms mixing time).

Protons *b* and *c* show NOEs with aryl side-group protons *e* and *e'* (Figure S20). The cross peak between protons *e* and *e'* probably arises from chemical exchange (rotation of the aryl groups, which is slow on the chemical shift timescale). Protons *a*, *b*, *c*, *d*, *e* and *e'*, which are all on the 12-porphyrin nanoring, show NOEs with a signal at 1.57 ppm. This must correspond to the *tert*-butyl groups on *c*-P12. This *t*-Bu¹² group also has a NOE with aryl side-group proton *f* (Figure S21).

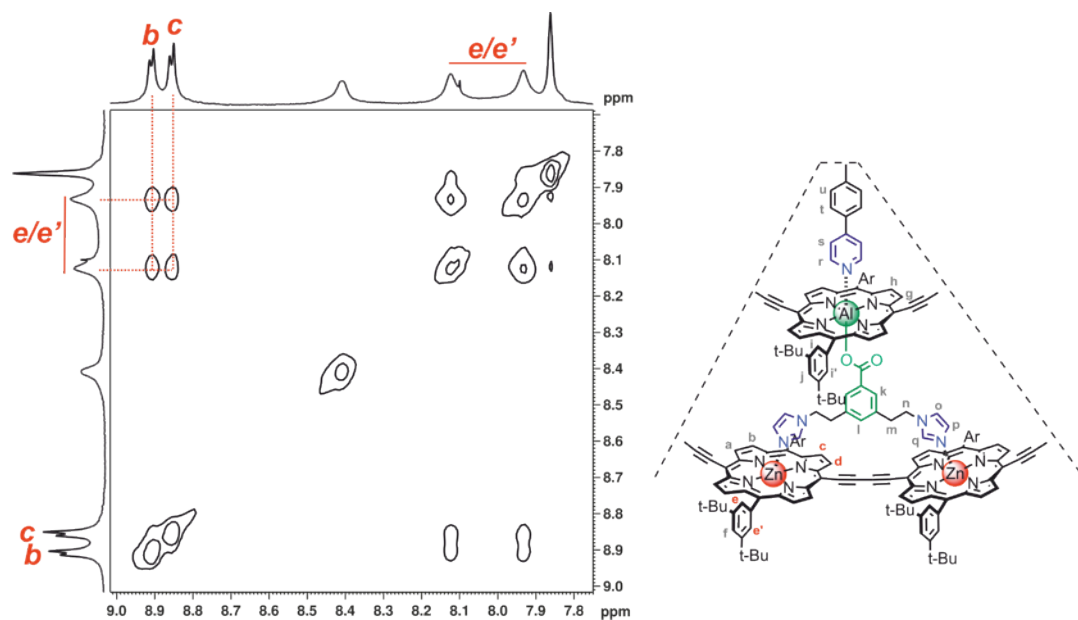


Figure S20. Region of the NOESY spectrum of **T6•c-P6•(L1)₆•c-P12** corresponding to the β-protons in *c*-P12 and the aryl side-group protons (400 MHz, CD₂Cl₂, 298 K, 300 ms mixing time).

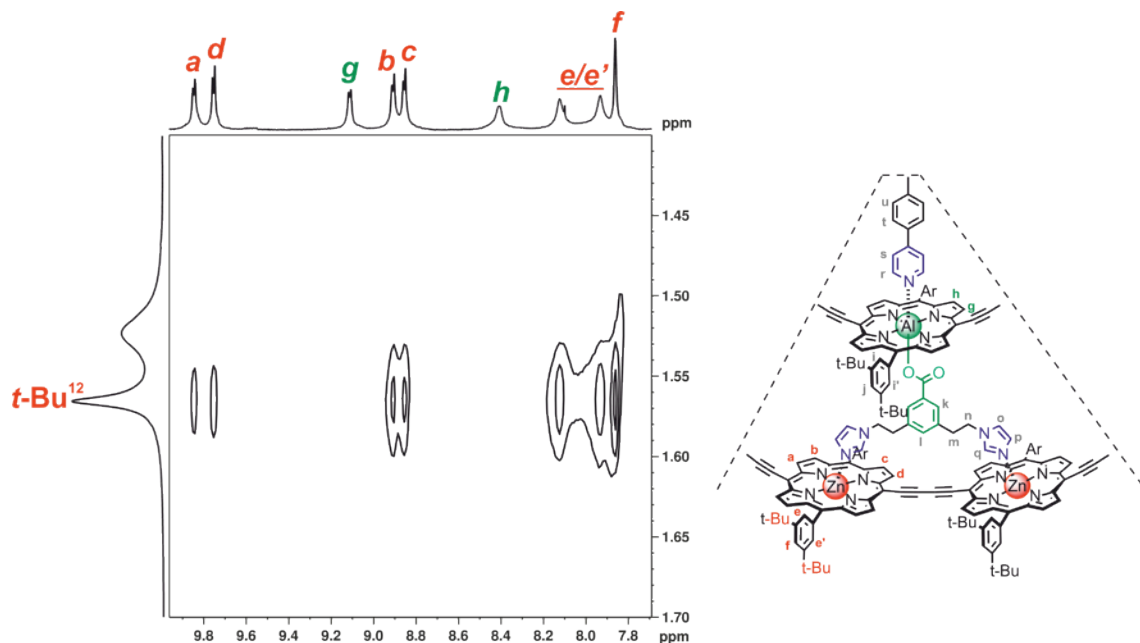


Figure S21. Region of the NOESY spectrum of **T6•c-P6•(L1)₆•c-P12** corresponding to the β-protons, the aryl side-group protons and the *tert*-butyl protons (400 MHz, CD₂Cl₂, 298 K, 300 ms mixing time).

In the HSQC spectrum, protons *e* and *e'* correlate with signals at 129.7 and 130.1 ppm (Figure S22). Proton *f* correlates with a signal at 121.0 ppm and the other proton that correlates with a signal at 121.4 ppm must be *para*-proton *j* from *c*-P6.

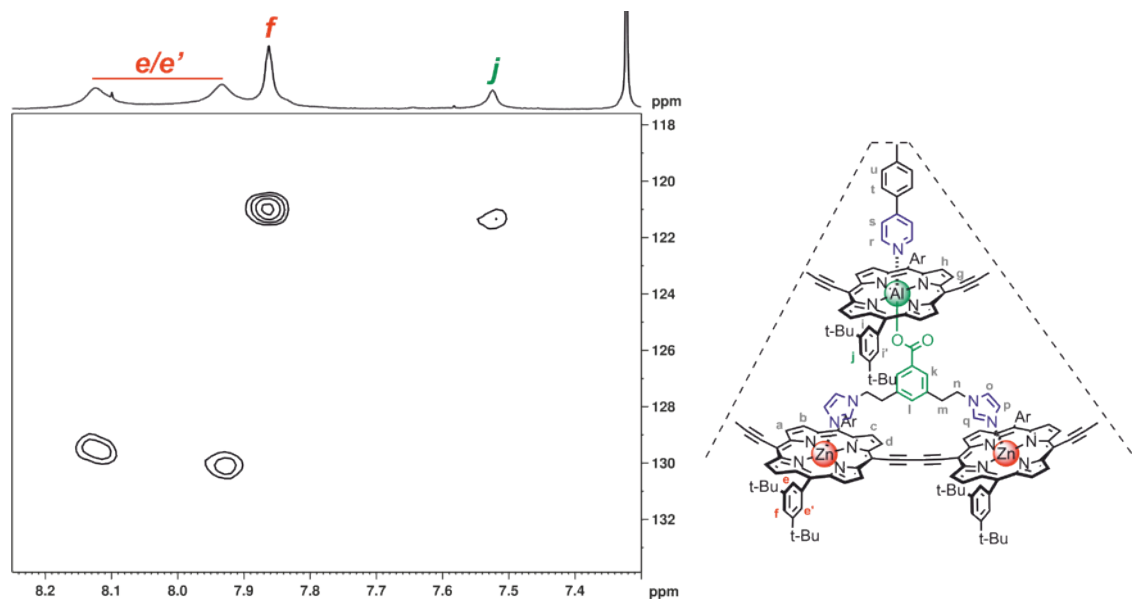


Figure S22. Region of the HSQC spectrum of $\text{T6}\cdot\text{c-P6}\cdot(\text{L1})_6\cdot\text{c-P12}$ corresponding to aryl side-group protons in *c*-P12 and *c*-P6 (400 MHz, CD_2Cl_2 , 298 K).

Proton *j* shows a NOE with *tert*-butyl protons $t\text{-Bu}^6$ (Figure S23), which unlike $t\text{-Bu}^{12}$ are non-equivalent in *c*-P6 and in slow-exchange based on the ROESY spectrum. Protons $t\text{-Bu}^6$ also show NOEs to protons *g* and *h* on *c*-P6 (Figure S24).

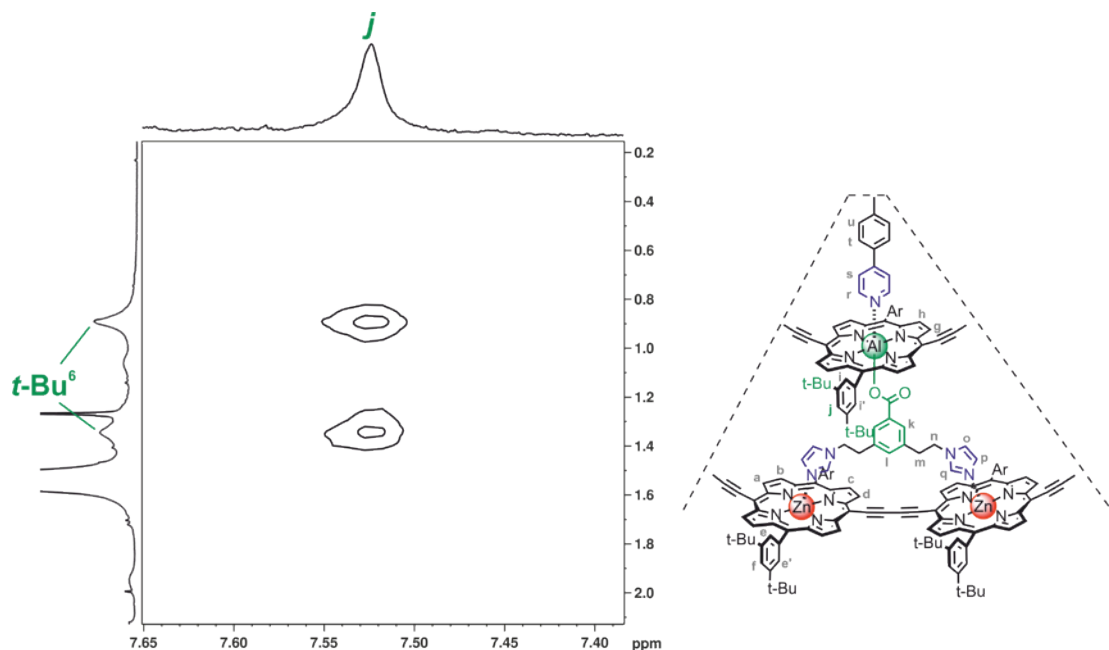


Figure S23. Region of the NOESY spectrum of $\text{T6}\cdot\text{c-P6}\cdot(\text{L1})_6\cdot\text{c-P12}$ corresponding to proton *j* and the *tert*-butyl protons in *c*-P6 (400 MHz, CD_2Cl_2 , 298 K, 300 ms mixing time).

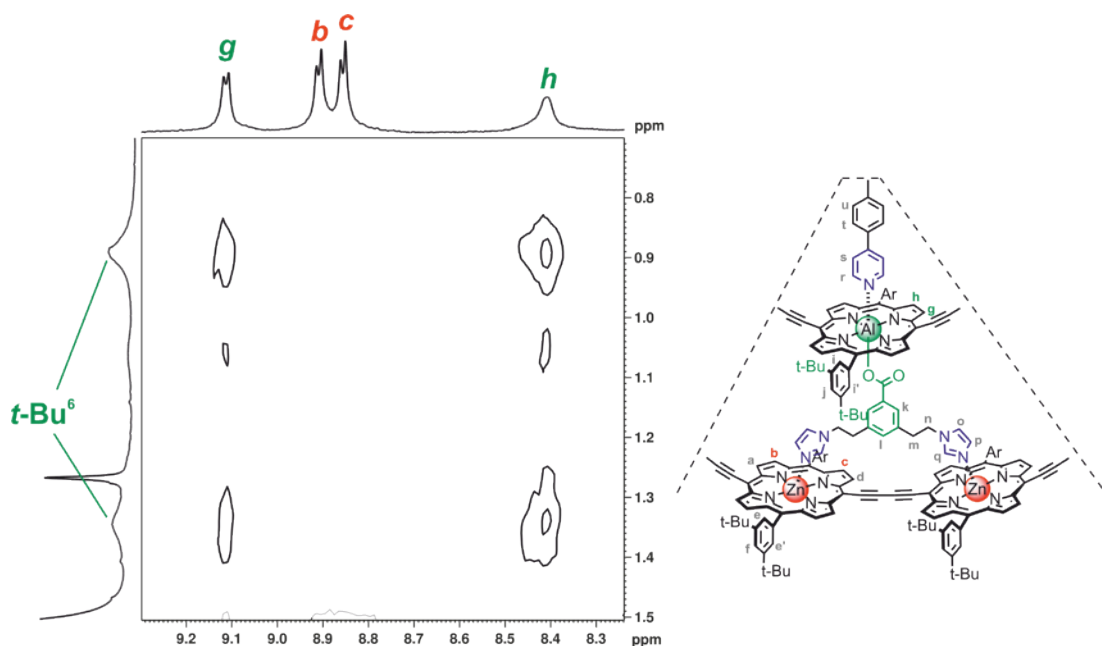


Figure S24. Region of the NOESY spectrum of $T6 \bullet c-P6 \bullet (L1)_6 \bullet c-P12$ corresponding to the β -protons and the *tert*-butyl protons in *c-P6* (400 MHz, CD_2Cl_2 , 298 K, 300 ms mixing time).

From the ROESY spectrum, the assignment of *ortho* aryl protons *e* and *e'* in *c-P12* is confirmed. They are in slow exchange on the NMR time scale. A second set of signals in slow exchange can be seen in the same chemical shift range. These must correspond to *ortho* aryl protons *i* and *i'* in *c-P6*. Proton *i'* also shows a NOE to β -proton *h* (Figure S25).

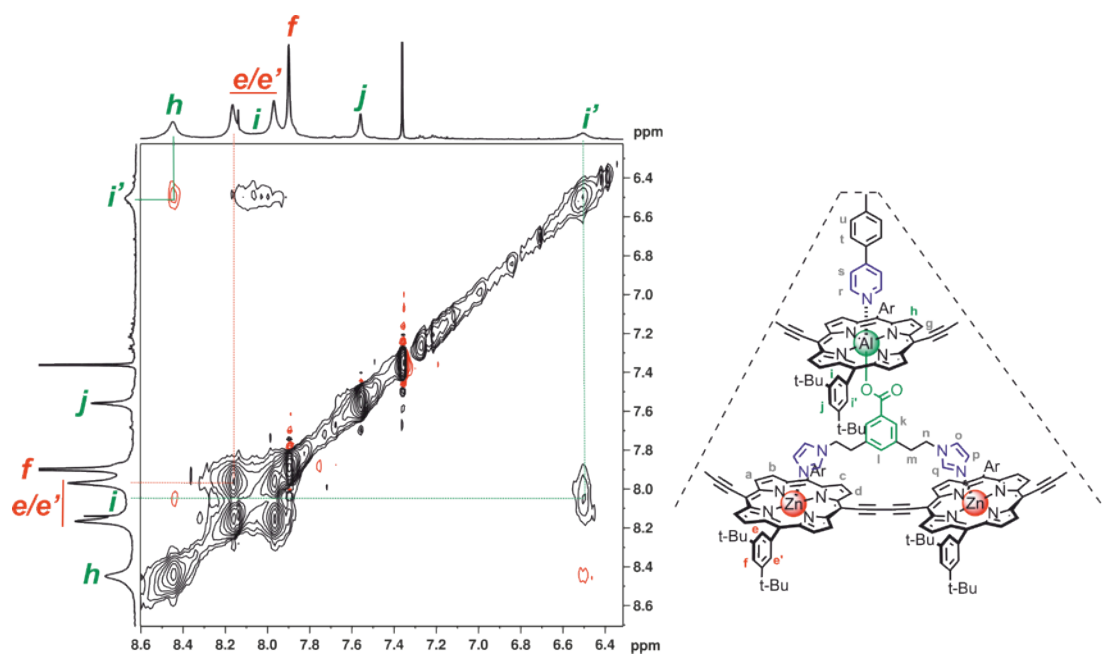


Figure S25. Region of the ROESY spectrum of $T6 \bullet c-P6 \bullet (L1)_6 \bullet c-P12$ corresponding to the aryl side-group protons in *c-P12* and *c-P6* (500 MHz, CD_2Cl_2 , 298 K, 300 ms mixing time).

The assignment of aryl protons *i* and *i'* was confirmed in the NOESY spectrum. NOEs are observed between protons *g* and *i/i'* as well as protons *h* and *i/i'* (Figure S26). A weak NOE is also observed between protons *h* and *j*.

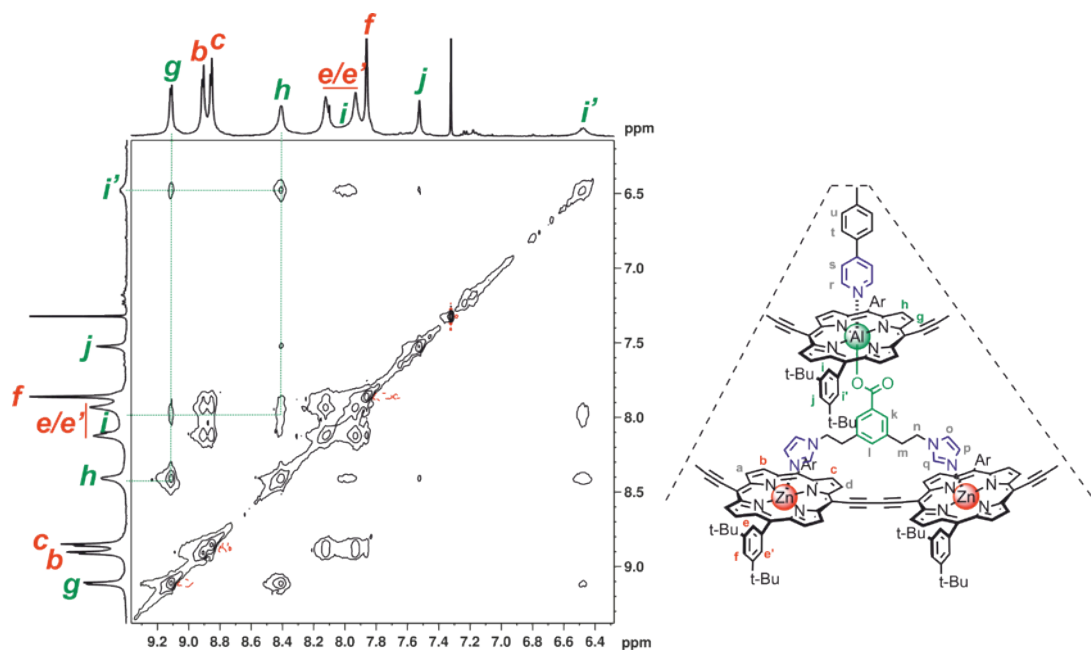


Figure S26. Region of the NOESY spectrum of $T6 \bullet c\text{-}P6 \bullet (L1)_6 \bullet c\text{-}P12$ corresponding to the β -protons and the aryl side-group protons in *c*-P6 (400 MHz, CD_2Cl_2 , 298 K, 300 ms mixing time).

Having assigned all of the porphyrin protons in the Russian doll, we next turned our attention to the bridging ligand protons in this system. Protons *m* and *n* were the clearest to identify, based on their strong coupling in the COSY spectrum. These protons also correlated with signals in the HSQC spectrum corresponding to CH_2 groups. Based on the chemical shifts in the HSQC, proton *n* corresponds to the signal at 1.95 ppm (correlates to CH_2 group at 46.8 ppm in the HSQC) and proton *m* corresponds to the signal at 1.06 ppm (correlates to CH_2 group at 35.1 ppm in the HSQC) (Figure S27).

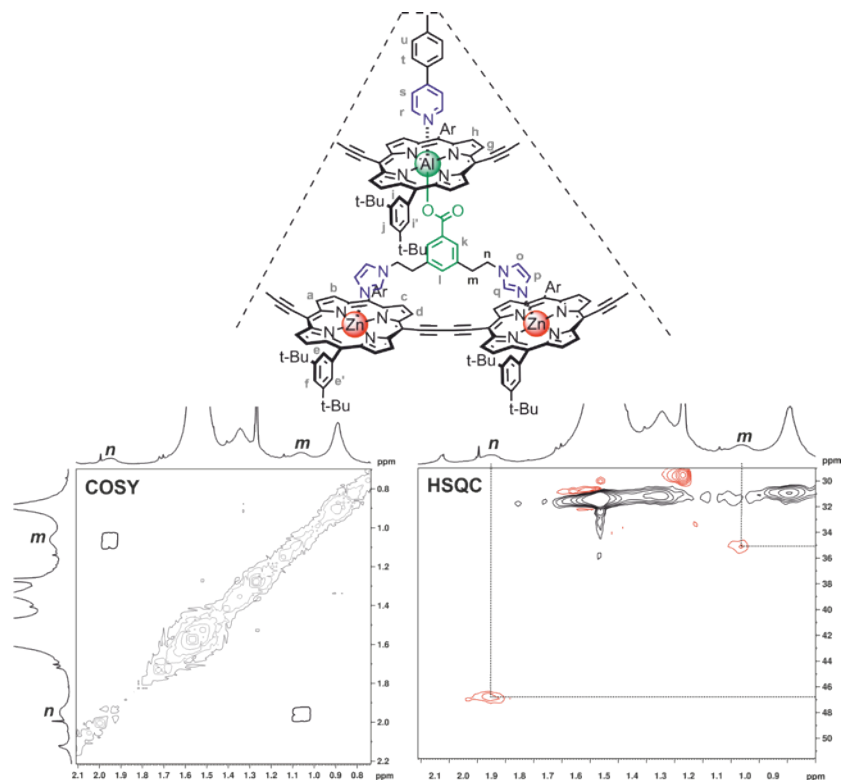


Figure S27. Regions of the COSY and HSQC spectra of $T6 \bullet c-P6 \bullet (L1)_6 \bullet c-P12$ corresponding to the bridging ligand protons m and n (400 MHz, CD_2Cl_2 , 298 K).

In the NOESY spectrum, protons m and n show strong NOEs to proton k or l (Figure S28). There is also a weak NOE between proton k (or l) and $t-Bu^6$.

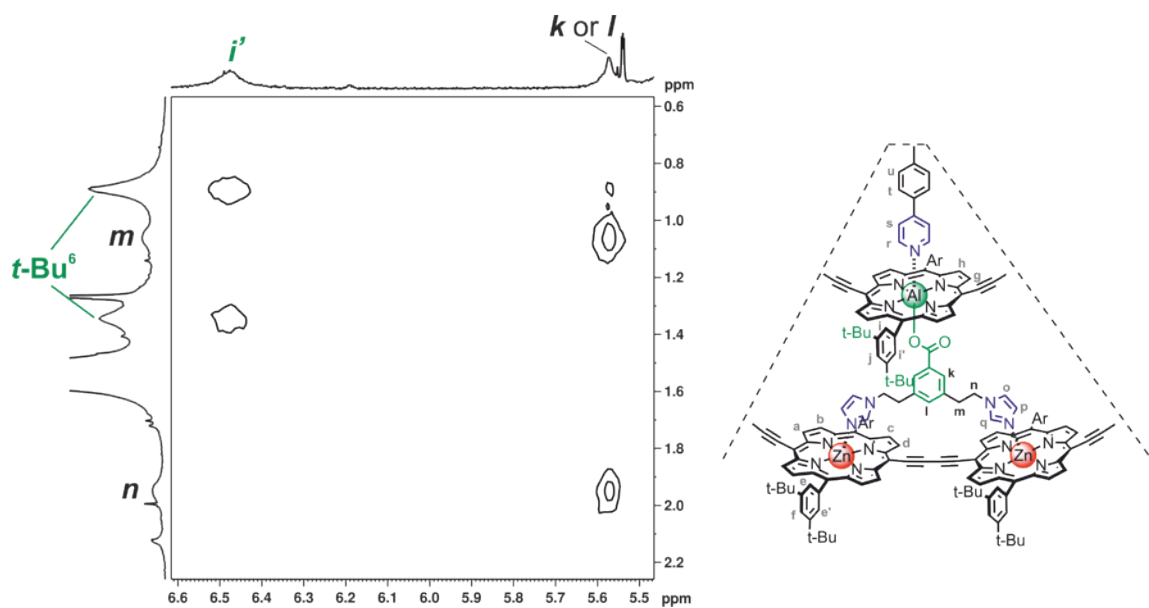


Figure S28. Region of the NOESY spectrum of $T6 \bullet c-P6 \bullet (L1)_6 \bullet c-P12$ corresponding to the bridging ligand protons m , n and k (or l) (400 MHz, CD_2Cl_2 , 298 K, 300 ms mixing time).

Due to ring-current effects, the imidazole protons *p* and *q* in the bridging ligand are shielded and appear at low chemical shift. Proton *p* was assigned based on its NOE with the *c*-**P12** β-protons *a* and *b* (Figure S29). Proton *p* correlates with proton *o* (at 4.88 ppm) in the COSY spectrum. Proton *o* shows strong NOEs to protons *m*, *n* and *p*.

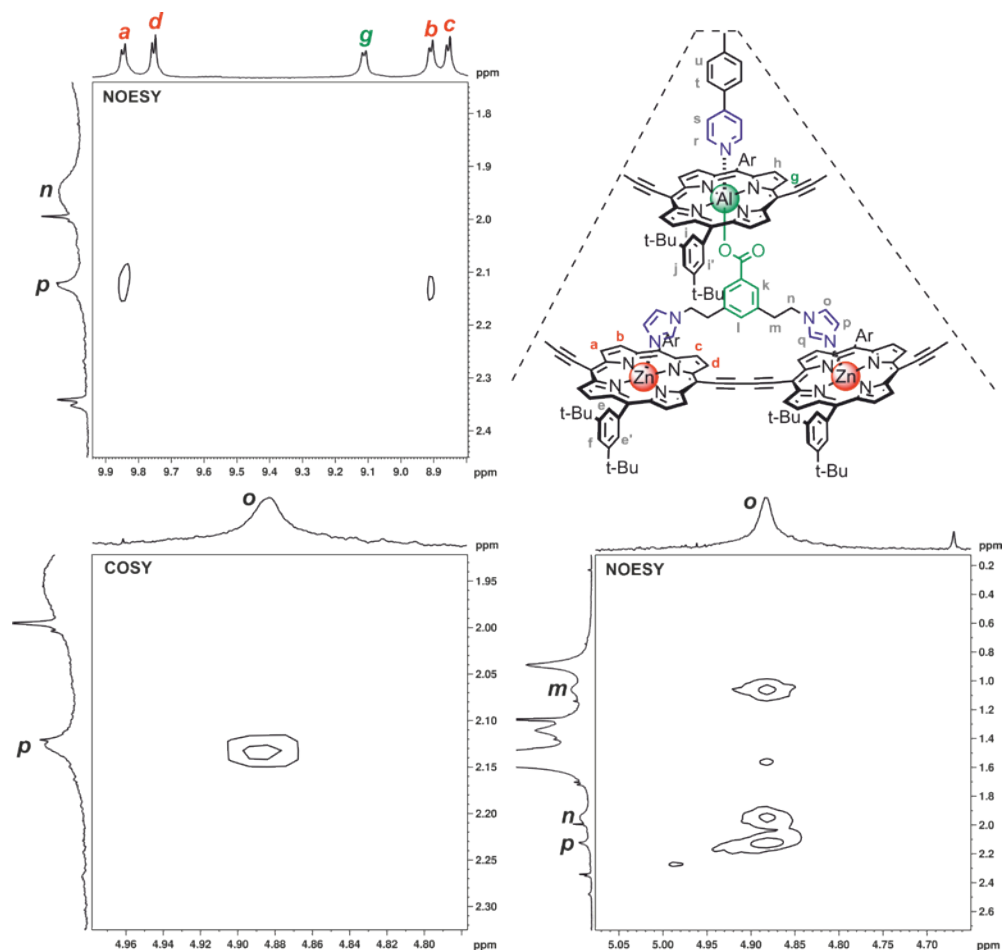


Figure S29. Regions of the COSY and NOESY spectra of **T6•c-P6•(L1)₆•c-P12** corresponding to the bridging ligand protons *m*, *n*, *o* and *p*, and the β-protons *a* and *b* (400 MHz, CD₂Cl₂, 298 K, 300 ms mixing time for NOESY).

Hexapyridyl template **T6** protons *t* and *u* were assigned to the multiplet at 5.42 ppm based on the assignments made for **T6•c-P6•(Ar'CO₂)₆** in the previous section. This was supported by the HSQC spectrum, which shows a correlation between *t* and *u* and signals at 130.5 and 123.7 ppm, respectively (Figure S30). These chemical shifts are in agreement with previously reported nanoring-**T6** systems.

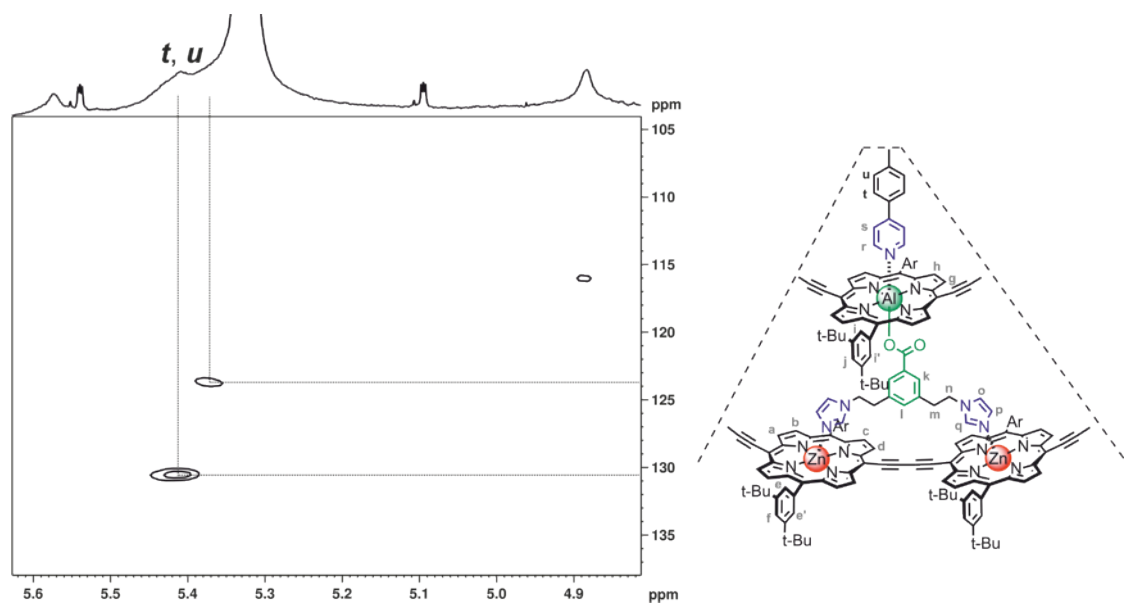


Figure S30. Region of the HSQC spectrum of **T6•c-P6•(L1)₆•c-P12** corresponding to template **T6** protons *t* and *u* (400 MHz, CD₂Cl₂, 298 K).

Similar to observations made for the imidazole protons *p* and *q*, the α -pyridyl proton *r* in **T6** is shielded and appears at very low chemical shift due to ring-current effects. Proton *r* was assigned based on the presence of weak NOEs between *c-P6* protons *g* and *h* and a proton at 1.55 ppm (Figure S31). Proton *r* also has a NOE with proton *s* at 4.88 ppm (Figure S32). These assignments correlate nicely with the assignments made for **T6•c-P6•(Ar'CO₂)₆** in the previous section and with previously reported nanoring-**T6** system.

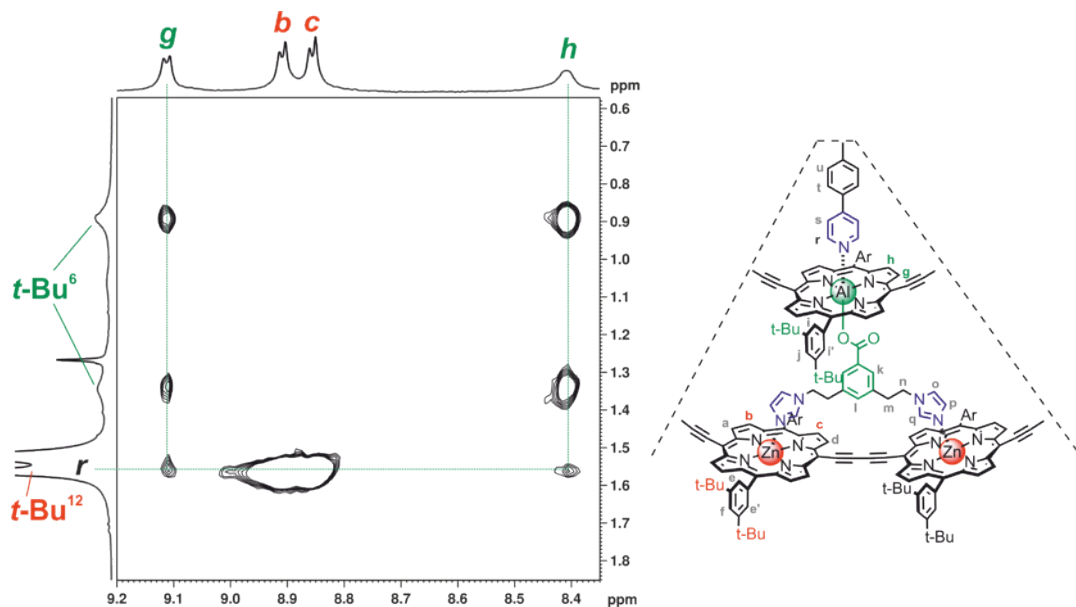


Figure S31. Region of the NOESY spectrum of **T6•c-P6•(L1)₆•c-P12** corresponding to template **T6** proton *r* and *c-P6* β -protons *a* and *b* (400 MHz, CD₂Cl₂, 298 K, 300 ms mixing time).

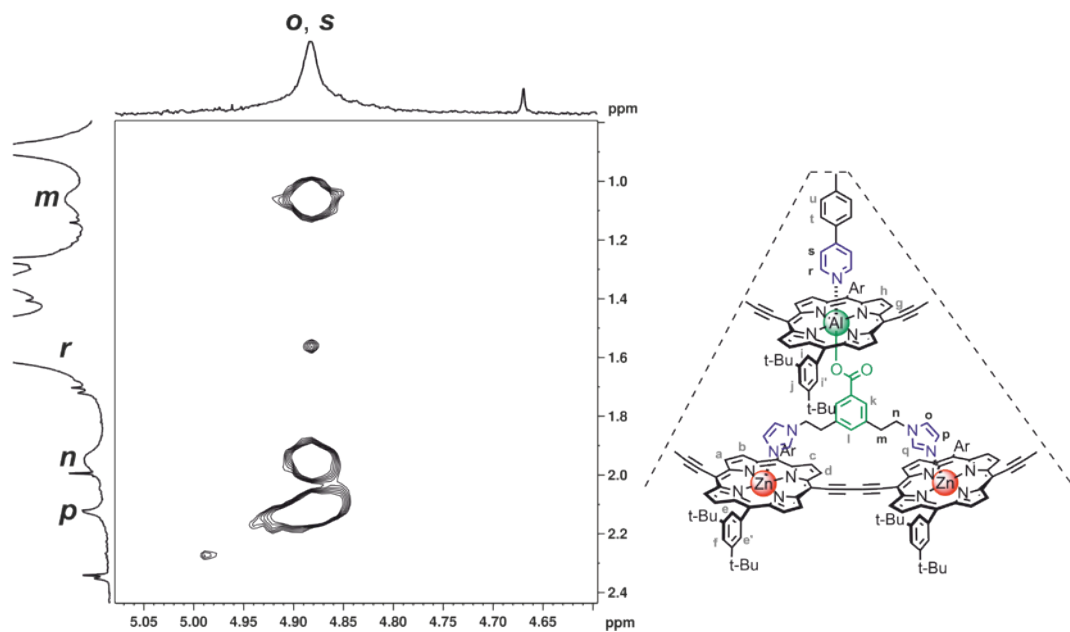


Figure S32. Region of the NOESY spectrum of **T6•c-P6•(L1)₆•c-P12** corresponding to template **T6** protons *r* and *s* (400 MHz, CD₂Cl₂, 298 K, 300 ms mixing time).

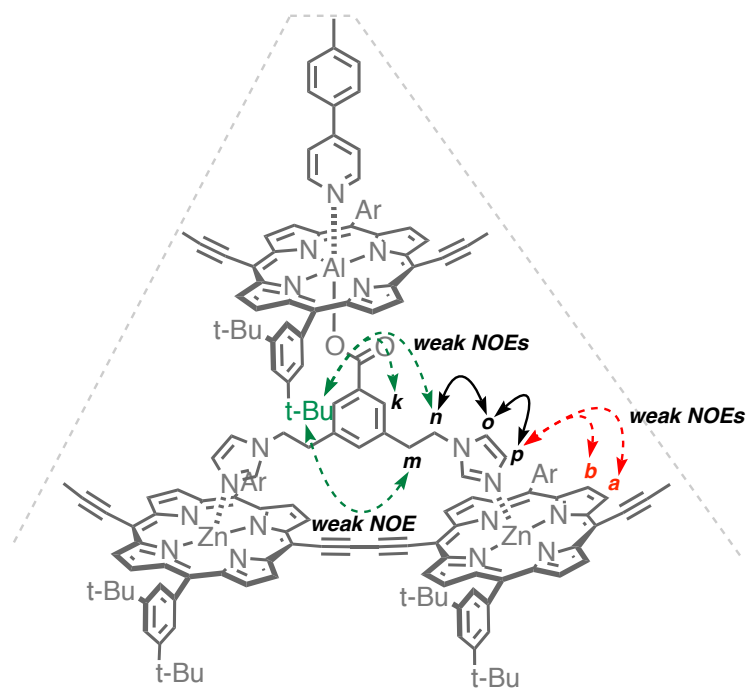


Figure S33. NOE pathway observed between the outer 12-porphyrin nanoring and inner 6-porphyrin nanoring. NOEs are observed between protons from i) the bridging ligand (black), ii) the outer ring and the bridging ligand (red), and iii) the inner ring and the bridging ligand (green).

D4) Change in chemical shift for protons in *c*-P12, T6•*c*-P6•(Ar'CO₂)₆ and ligand L1 upon formation of the Russian doll complex

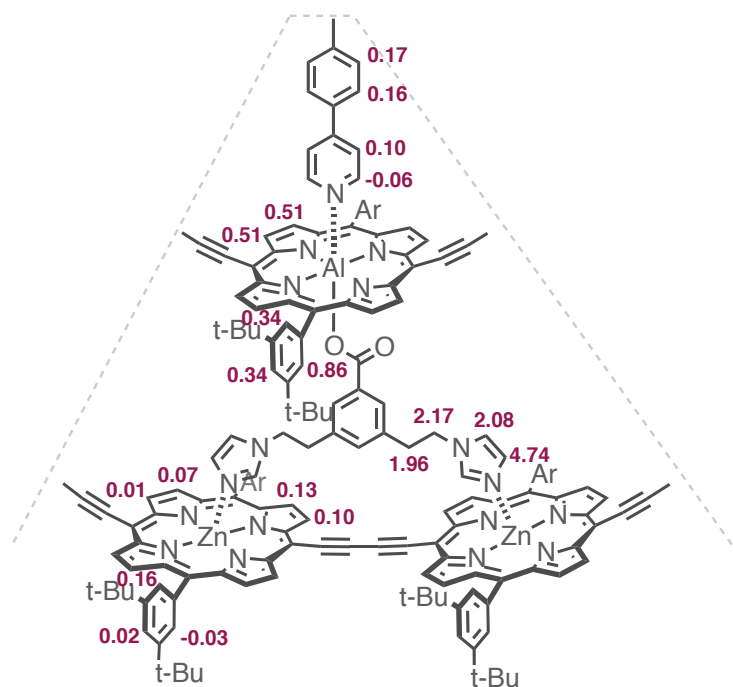


Figure S34. Changes in the chemical shift ($\Delta\delta$) in the ¹H NMR of *c*-P12, T6•*c*-P6•(Ar'CO₂)₆ and ligand L1 upon formation of the Russian doll complex (CD₂Cl₂, 298K). The $\Delta\delta$ was calculated from $\delta_{\text{free}} - \delta_{\text{bound}}$.

E. Binding Studies

E1) Denaturation Titration of $c\text{-P12}\cdot(\text{Bn-L1})_6$ with Quinuclidine

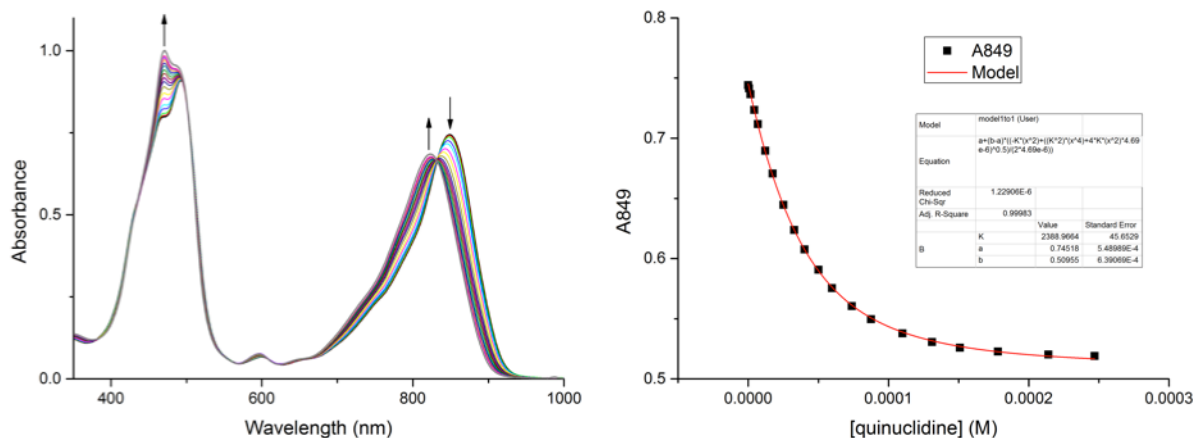
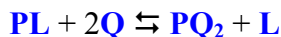


Figure S35. UV/vis/NIR titration of $c\text{-P12}\cdot(\text{Bn-L1})_6$ ($[c\text{-P12}\cdot(\text{Bn-L1})_6] = 7.82 \times 10^{-7}$ M) with quinuclidine in CHCl_3 at 298 K. a) Changes in absorption upon addition of quinuclidine. Arrows indicate areas of increasing and decreasing absorption during the titration; b) Binding isotherm (black squares) derived from absorption data at $\lambda = 849$ nm and calculated fit from Origin (red line) giving $K_{\text{dn}} = (2.39 \pm 0.05) \times 10^3 \text{ M}^{-1}$.

The titration of $c\text{-P12}\cdot(\text{Bn-L1})_6$ with quinuclidine **Q** was analyzed assuming that each **Bn-L1** unit binds independently, so that the equilibrium can be treated as the displacement of a 2-site ligand **L** from a 2-site receptor **P**, with the initial concentration of **PL** being, $[\text{P}]_0$, six times the concentration of $c\text{-P12}\cdot(\text{Bn-L1})_6$.



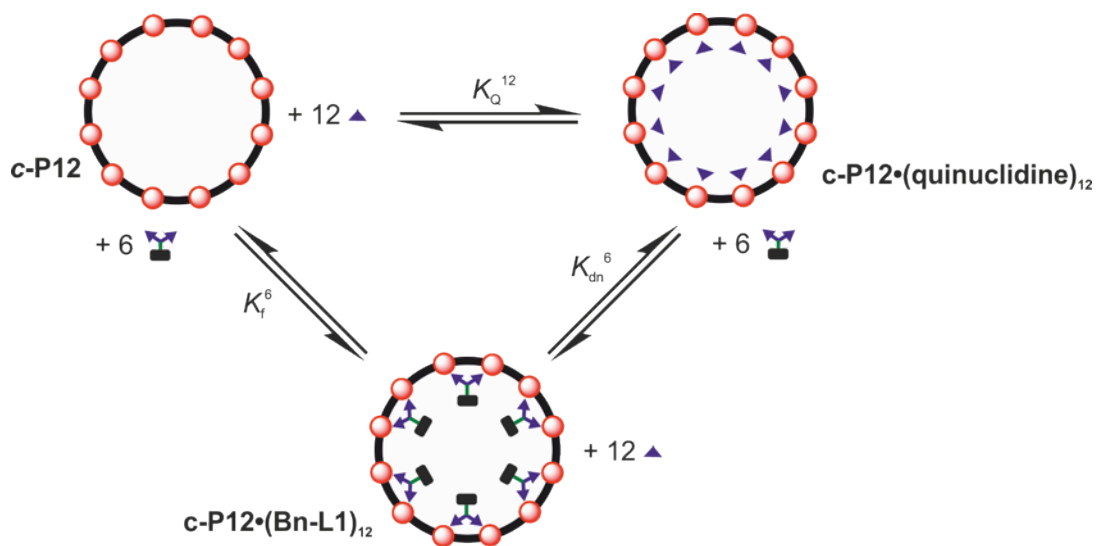
$$K_{\text{dn}} = \frac{[\text{PQ}_2][\text{L}]}{[\text{Q}]^2[\text{PL}]} \quad (\text{S1})$$

The denaturation equilibrium constant, K_{dn} , defined by equation (S1) was determined by fitting the binding isotherm to equation (S2), from ref. S11,

$$\frac{A - A_0}{A_f - A_0} = \frac{-K_{\text{dn}}[\text{Q}]^N + \sqrt{K_{\text{dn}}^2[\text{Q}]^{2N} + 4K_{\text{dn}}[\text{Q}]^N[\text{P}]_0}}{2[\text{P}]_0} \quad (\text{S2})$$

where A is the absorption at any point in the titration, A_0 is the initial absorption, A_f is the final absorption, N is the number of binding sites ($N = 2$), $[\text{Q}]$ is the total concentration of quinuclidine at each point in the titration and $[\text{P}]_0$ is $[c\text{-P12}\cdot(\text{Bn-L1})_6]/6$.

The average value of K_{dn} obtained from fitting the binding isotherms at various wavelengths to a 2-site binding model for the break-up of $c\text{-P12}\cdot(\text{Bn-L1})_6$ is $K_{\text{dn}} = (2.5 \pm 0.2) \times 10^3 \text{ M}^{-1}$. To determine the 1:1 formation constant for $c\text{-P12}\cdot(\text{Bn-L1})_6$, the following thermodynamic cycle was used:



The addition of excess quinuclidine results in the displacement of the ligand **Bn-L1** from **c-P12**, to generate **c-P12•(quinuclidine)₁₂**. With the values of $K_{dn} = (2.5 \pm 0.2) \times 10^3 \text{ M}^{-1}$ and $K_Q = (1.0 \pm 0.2) \times 10^5 \text{ M}^{-1}$, K_f can be calculated using equation (S3),

$$K_f = \frac{K_Q^2}{K_{dn}} \quad (\text{S3})$$

which gives $\log K_f = 6.6 \pm 0.1$.

E2) Denaturation Titration of $\text{T6}\cdot\text{c-P6}\cdot(\text{L1})_6\cdot\text{c-P12}$ with Quinuclidine

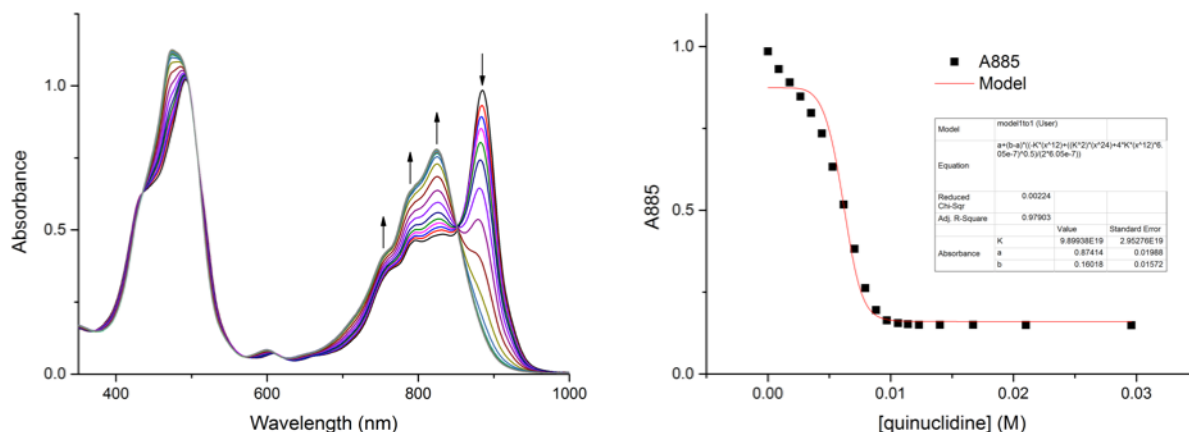
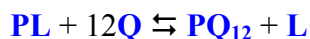


Figure S36. UV/vis/NIR titration of $\text{T6}\cdot\text{c-P6}\cdot(\text{L1})_6\cdot\text{c-P12}$ ($[\text{T6}\cdot\text{c-P6}\cdot(\text{L1})_6\cdot\text{c-P12}] = 6.05 \times 10^{-7} \text{ M}$) with quinuclidine in CHCl_3 at 298 K. a) Changes in absorption upon addition of quinuclidine. Arrows indicate areas of increasing and decreasing absorption during the titration. b) Binding isotherm (black squares) derived from absorption data at $\lambda = 885 \text{ nm}$ and calculated fit from Origin (red line) giving $K_{\text{dn}} = (9.9 \pm 3.0) \times 10^{19} \text{ M}^{-11}$.

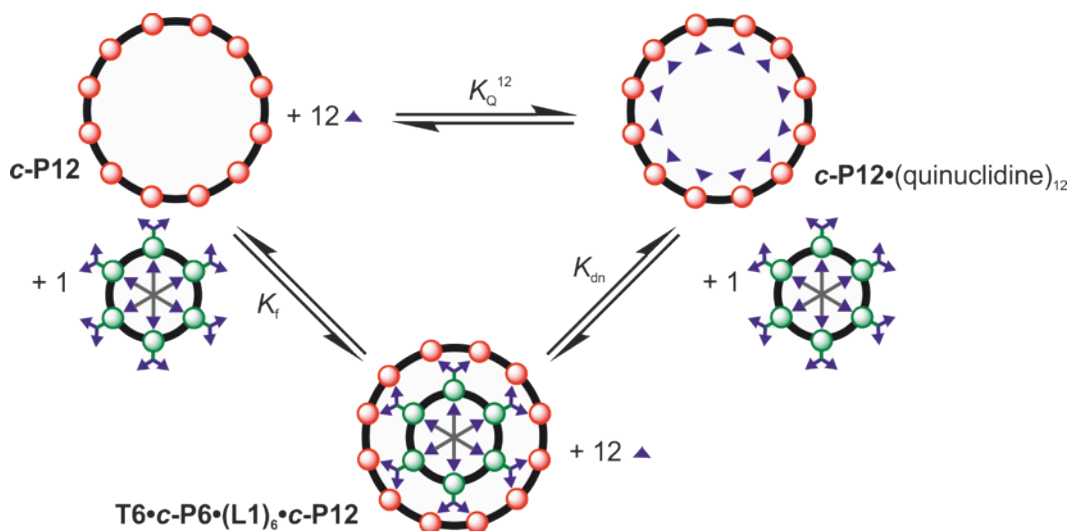
The titration of $\text{T6}\cdot\text{c-P6}\cdot(\text{L1})_6\cdot\text{c-P12}$ with quinuclidine **Q** was analyzed as a two-state equilibrium, where **PL** is $\text{T6}\cdot\text{c-P6}\cdot(\text{L1})_6\cdot\text{c-P12}$ and **L** is $\text{T6}\cdot\text{c-P6}\cdot(\text{L1})_6$:



$$K_{\text{dn}} = \frac{[\text{PQ}_{12}][\text{L}]}{[\text{Q}]^{12}[\text{PL}]} \quad (\text{S4})$$

The denaturation equilibrium constant, K_{dn} , defined by equation (S4) was determined by fitting the binding isotherm to equation (S2) with $N = 12$.

The average value of K_{dn} obtained from fitting the binding isotherms at various wavelengths to this 12-site binding model is $K_{\text{dn}} = (9.6 \pm 3.0) \times 10^{19} \text{ M}^{-11}$. To determine the 1:1 formation constant for $\text{T6}\cdot\text{c-P6}\cdot(\text{L1})_6\cdot\text{c-P12}$, the following thermodynamic cycle was used:



The addition of excess quinuclidine results in the displacement of **T6•c-P6•(L1)₆** from **c-P12**, to generate **c-P12•(quinuclidine)₁₂**. At these concentrations of quinuclidine, **T6** is not displaced from **T6•c-P6•(Ar'CO₂)₆**. With the values of $K_{\text{dn}} = (9.6 \pm 3.0) \times 10^{19} \text{ M}^{-11}$ and $K_{\text{Q}} = (1.0 \pm 0.2) \times 10^5 \text{ M}^{-1}$, K_{f} can be calculated as follows:

$$K_{\text{f}} = \frac{K_{\text{Q}}^{12}}{K_{\text{dn}}}$$

$$\log K_{\text{f}} = 12 \log K_{\text{Q}} - \log K_{\text{dn}} \quad (\text{S5})$$

which gives $\log K_{\text{f}} = 40 \pm 1$.

E3) Calculation of Effective Molarity

The effective molarity can be calculated using equation (S6),

$$\overline{\text{EM}} = \sqrt[N-1]{\frac{K_{\text{f}}}{K_{\sigma} K_1^N}}$$

$$\log \overline{\text{EM}} = \frac{\log K_{\text{f}} - \log K_{\sigma} - N \log K_1}{(N - 1)} \quad (\text{S6})$$

where K_{f} is the equilibrium constant for binding of **c-P12** with **T6•c-P6•(L1)₆**, K_{σ} is a statistical factor, K_1 is the microscopic binding constant of the corresponding reference ligand **Bn-L1** in **c-P12•(Bn-L1)₆** and N is the number of binding sites ($N = 6$).

The statistical factor was calculated as shown in Figure S37.

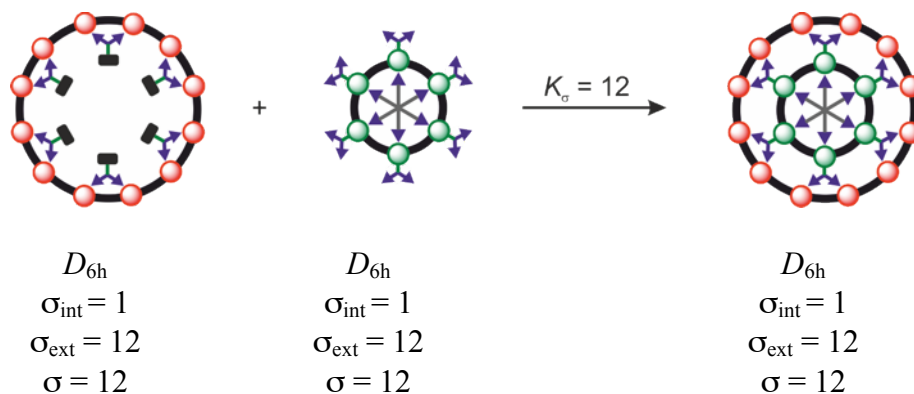


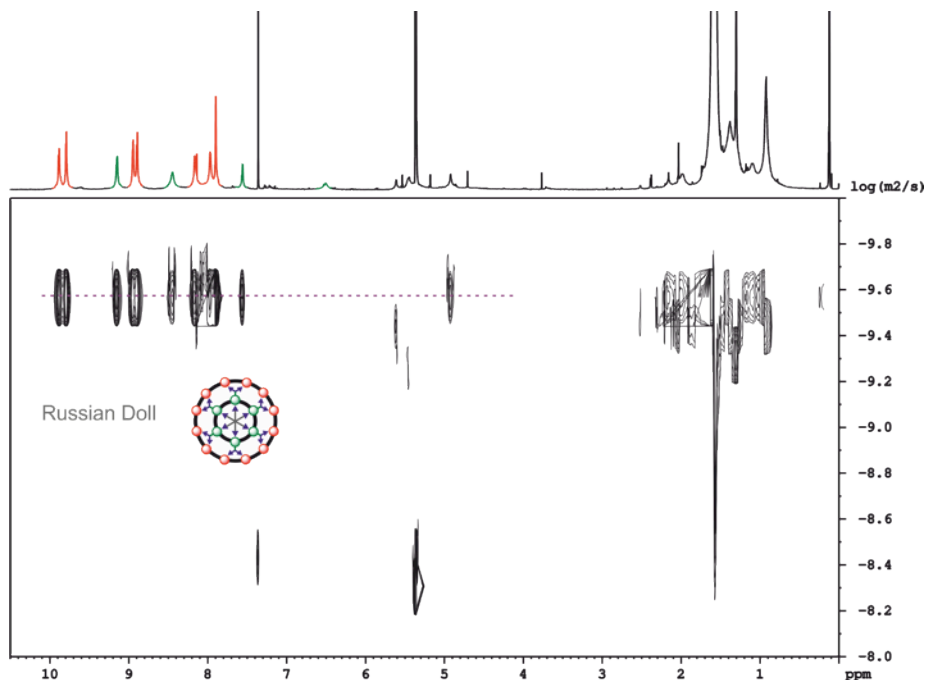
Figure S37. Statistical factors for **T6•c-P6•(L1)₆•c-P12**.

With the values of $\log K_1 = 6.6 \pm 0.1$, $\log K_{\text{f}} = 40 \pm 1$, $K_{\sigma} = 12$, and $N = 6$, the average effective molarity for Russian doll formation is given by $\log \overline{\text{EM}} = -0.13 \pm 0.23$, which means that the effective molarity is in the range 1.3 to 0.4 M.

F. DOSY NMR Experiments

F1) Russian Doll

a)



b)

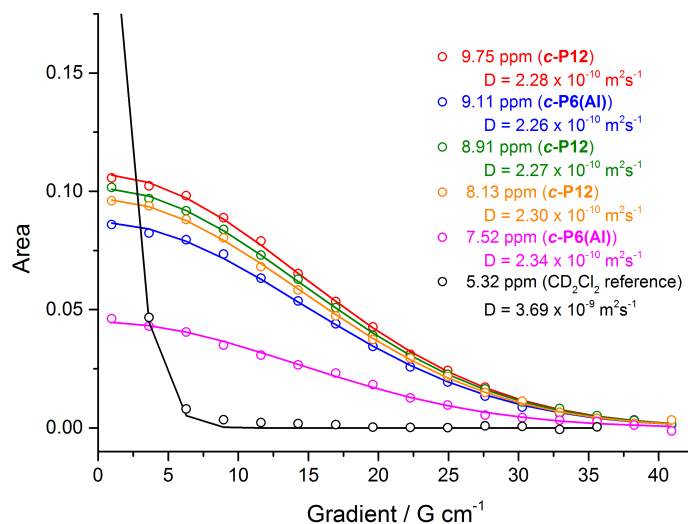
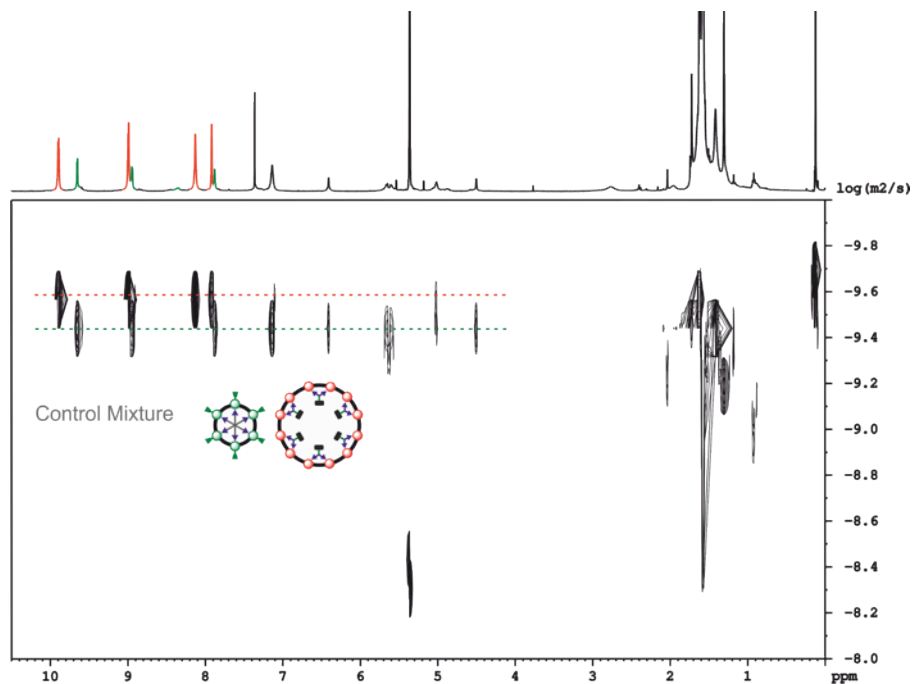


Figure S38. ¹H-DOSY of the Russian doll complex in CD₂Cl₂ at 298 K measured at 500 MHz with $\Delta = 100$ ms, $\delta = 4$ ms and $g = 0.96\text{--}41$ G cm⁻¹. a) DOSY plot (made using TOPSPIN software version 3.1). Protons corresponding to the larger 12-porphyrin nanoring are highlighted in red and protons corresponding to the smaller 6-porphyrin nanoring are highlighted in green. b) Fitted diffusion decay curves and resulting diffusion coefficients for selected protons of the large and small nanoring in the Russian doll complex. The diffusion coefficient for the complex, based on the average diffusion coefficients of these protons, is $D = (2.29 \pm 0.03) \times 10^{-10}$ m²/s.

F2) Control Mix

a)



b)

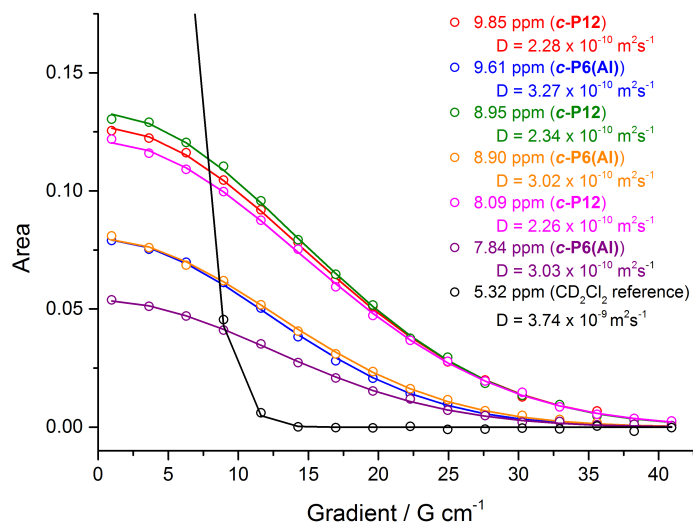


Figure S39. ¹H-DOSY of the *control mix* in CD₂Cl₂ at 298 K measured at 500 MHz with $\Delta = 100$ ms, $\delta = 4$ ms and $g = 0.96\text{--}41$ G cm⁻¹. a) DOSY plot (made using TOPSPIN software version 3.1). Protons corresponding to the larger 12-porphyrin nanoring are highlighted in red and protons corresponding to the smaller 6-porphyrin nanoring are highlighted in green. b) Fitted diffusion decay curves and resulting diffusion coefficients for selected protons of the large and small nanorings in the *control mix*. The diffusion coefficient for *c-P12*, based on the average diffusion coefficients of its protons, is $D = (2.29 \pm 0.03) \times 10^{-10}$ m²/s and the diffusion coefficient for **T6•c-P6•(Ar'CO₂)₆**, based on the average diffusion coefficients of its protons, is $D = (3.11 \pm 0.12) \times 10^{-10}$ m²/s.

G. Photophysics

G1) Absorption Spectra

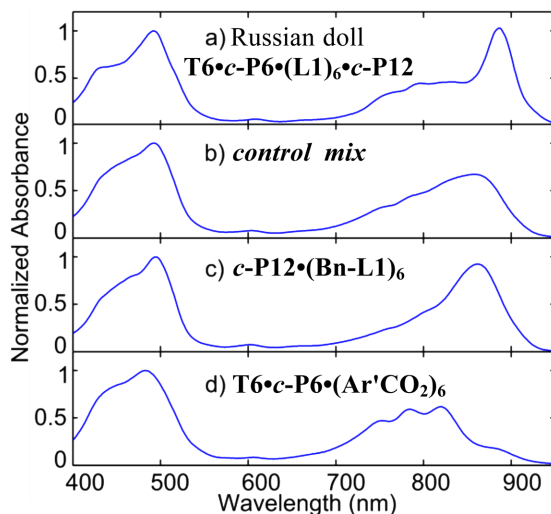


Figure S40. Normalized steady-state absorption spectra for (a) Russian doll complex, $\text{T6}\cdot\text{c-P6}(\text{L1})_6\cdot\text{c-P12}$, (b) *control mix*, 1:1 $\text{c-P12}(\text{Bn-L1})_6$ and $\text{T6}\cdot\text{c-P6}(\text{Ar}'\text{CO}_2)_6$, (c) $\text{c-P12}(\text{Bn-L1})_6$ and (d) $\text{T6}\cdot\text{c-P6}(\text{Ar}'\text{CO}_2)_6$ recorded at 295 K in CHCl_3 .

Absorption spectra were recorded at room temperature for the Russian doll, the *control mix*, $\text{c-P12}(\text{Bn-L1})_6$ and $\text{T6}\cdot\text{c-P6}(\text{Ar}'\text{CO}_2)_6$ in CHCl_3 (Figure S40). All of the samples show a strong Soret band (400–550 nm) and a split Q band (700–950 nm). The Q band for the $\text{c-P12}(\text{Bn-L1})_6$ complex is red-shifted compared to $\text{T6}\cdot\text{c-P6}(\text{Ar}'\text{CO}_2)_6$ due to an increased conjugation length (Figure S40c,d). The absorption spectrum of the *control mix* consists of the sum of the contributions from its components, $\text{c-P12}(\text{Bn-L1})_6$ and $\text{T6}\cdot\text{c-P6}(\text{Ar}'\text{CO}_2)_6$, whereas the Russian doll shows a further red-shift in the Q band, due to the rigidity of the c-P12 component in the assembled complex.

G2) Fluorescence Spectra

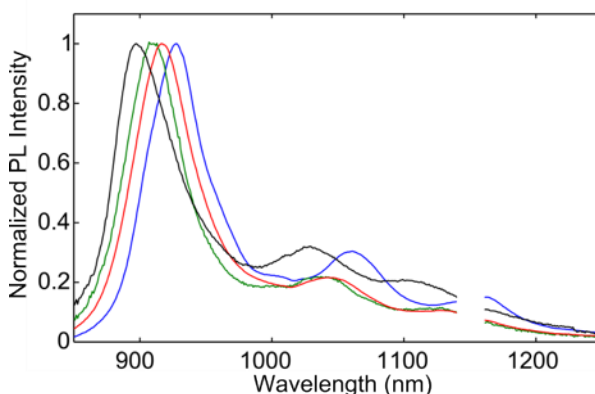


Figure S41. Normalized time-integrated fluorescence spectra of Russian doll complex, $\text{T6}\cdot\text{c-P6}(\text{L1})_6\cdot\text{c-P12}$ (blue), *control mix*, 1:1 $\text{c-P12}(\text{Bn-L1})_6$ and $\text{T6}\cdot\text{c-P6}(\text{Ar}'\text{CO}_2)_6$ (green), $\text{c-P12}(\text{Bn-L1})_6$ (red) and $\text{T6}\cdot\text{c-P6}(\text{Ar}'\text{CO}_2)_6$ (black) at 295 K in CHCl_3 recorded after excitation at 500 nm. (Data at 1142–1160 nm are distorted by a solvent absorption band and hence are omitted from the figure for clarity.)

Fluorescence spectra were measured at room temperature using a Horiba FluoroLog fluorometer for excitation in the Soret band at 500 nm. The fluorescence maxima of **T6•c-P6•(Ar'CO₂)₆** and **c-P12•(Bn-L1)₆** are observed at 897 nm and 917 nm, respectively. Both components contribute to the fluorescence in the *control mix*. As a result, the peak intensity of the *control mix* lies at 910 nm. The fluorescence spectrum of the Russian doll peaks at 928 nm, further red-shifted from **c-P12•(Bn-L1)₆** because the complex is more rigid than its unbound constituent components.

G3) Fluorescence Quantum Yields. The fluorescence quantum yields (Φ_F , i.e. the photoluminescence quantum efficiency) is calculated from the fluorescence intensity integrated over the entire spectrum and the absorbance at the excitation wavelength, with **l-P6** used as reference sample ($\Phi_F = 28\%$).^{S12} The quantum yield of **T6•c-P6•(Ar'CO₂)₆** ($\Phi_F = 2.1\%$) is lower than that of **c-P12•(Bn-L1)₆** ($\Phi_F = 8.4\%$), which is consistent with previous studies that have shown more strongly suppressed emission for smaller nanorings for which the excitonic wavefunction was delocalized over most of the ring.^{S12} Both components contribute to the fluorescence efficiency of the *control mix*, which lies in between, at $\Phi_F = 5.4\%$ (with excitation at 500 nm). The Russian doll has $\Phi_F = 2.4\%$, which is higher than that of **T6•c-P6•(Ar'CO₂)₆**, which could be attributed to energy transfer from the inner **c-P6** ring to the outer **c-P12** ring. The **c-P12** emission component in the Russian doll is more rigid than **c-P12•(Bn-L1)₆** resulting in the observed lowered Φ_F compared to **c-P12•(Bn-L1)₆**.

G4) Fluorescence Excitation Spectra

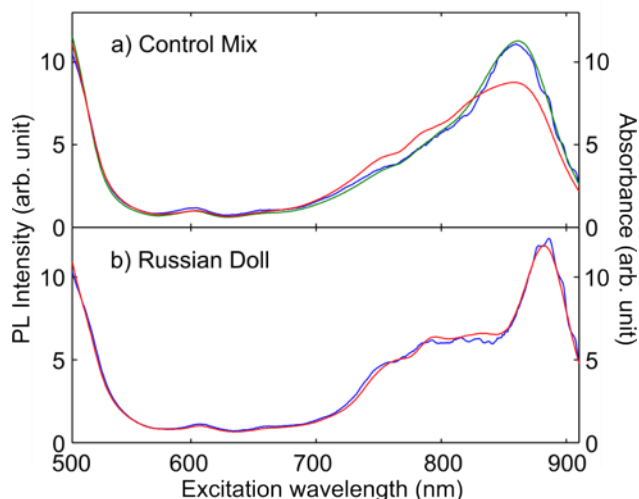


Figure S42. A comparison between the fluorescence excitation spectra detected at 929 nm (blue) and the absorption spectra (red) for (a) *control mix*, 1:1 **c-P12•(Bn-L1)₆** and **T6•c-P6•(Ar'CO₂)₆** and (b) Russian doll complex, **T6•c-P6•(L1)₆•c-P12**. The green curve in (a) is a simulation of the excitation spectrum calculated from the excitation-dependent fluorescence intensity using the absorption spectra of **T6•c-P6•(Ar'CO₂)₆** and **c-P12•(Bn-L1)₆**, weighted by the fluorescence quantum yields of the components.

The *control mix* comprises two emitting species, and for each emitter the fluorescence excitation is proportional to its absorption spectrum. While the absorption spectrum of the *control mix* is a sum of the contributions from the two components according to their amount, the fluorescence intensity also depends on the quantum yield of each component. As the Φ_F of **c-P12•(Bn-L1)₆** is much higher than that of **T6•c-P6•(Ar'CO₂)₆**, the excitation spectrum of the *control mix* is not expected to be proportional to its absorption spectrum. For the *control mix*, the calculated

excitation spectrum based on the measured absorption spectra and the Φ_F of **T6•c-P6•(Ar'CO₂)₆** and **c-P12•(Bn-L1)₆** agrees well with the experimentally determined excitation spectrum, as shown in Figure S42a. The absorption spectrum deviates from the excitation spectrum, especially at the red-edge of the Q band, as a result of the different fluorescence quantum yields of the components that make up the mix.

For the Russian doll, the excitation spectrum matches well with the absorption spectrum (Figure S42b), indicating that the whole complex acts as a single emitter, even though there are distinct features in the absorption spectrum arising from the different ring components. Evidently, there is energy transfer between the two porphyrin rings in the Russian doll complex.

G5) Measurement of Fluorescence Lifetimes

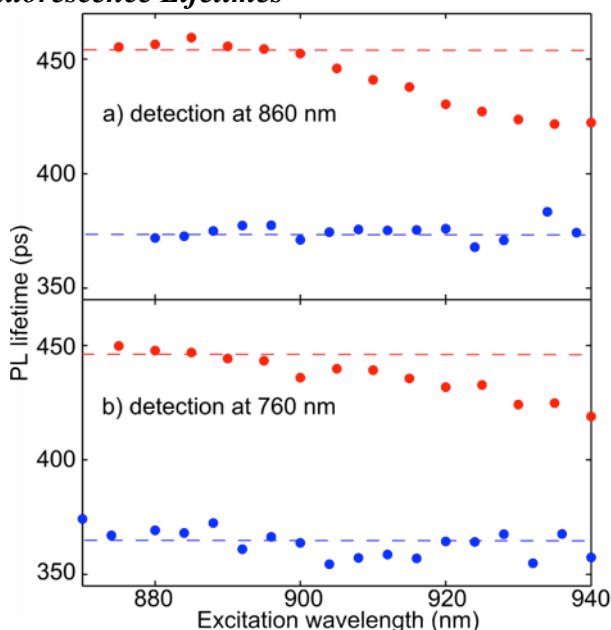
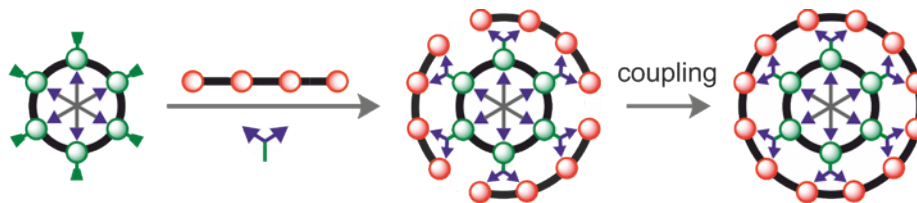


Figure S43. Excitation dependent fluorescence lifetime of the Russian doll **T6•c-P6•(L1)₆•c-P12** (blue) and the *control mix*, 1:1 **c-P12•(Bn-L1)₆** and **T6•c-P6•(Ar'CO₂)₆** (red) measured at detection wavelengths of (a) 860 nm and (b) 760 nm.

The fluorescence decay dynamics were investigated using the time-correlated single-photon counting (TCSPC) technique, and the fluorescence lifetime was extracted by fitting the experimental data to a single exponential decay model. The dependence of the fluorescence lifetime on the excitation wavelength was examined at two different detection wavelengths for the Russian doll and the *control mix* as shown in Figure S43. The fluorescence lifetimes of **T6•c-P6•(Ar'CO₂)₆** and **c-P12•(Bn-L1)₆** are 455 ps and 376 ps respectively, measured at a detection wavelength of 760 nm (not shown). The measured fluorescence lifetime for the *control mix* varies with increasing excitation wavelength from around 450 ps to 420 ps as the contribution from **T6•c-P6•(Ar'CO₂)₆** and **c-P12•(Bn-L1)₆** to the fluorescence changes with excitation wavelength. The fluorescence lifetime of the Russian doll, on the other hand, shows no dependence on excitation wavelength, indicating that the emission originates from a single emitter. The mean fluorescence lifetime of the Russian doll is 364 ps when detected at 760 nm and 375 ps when detected at 860 nm. A comparison with the individual component lifetimes suggests that the emitting species in the Russian doll is most likely the outer **c-P12**, suggesting fast energy transfer from **c-P6** within the time-resolution of the TCSPC system (40 ps).

H. Russian Doll Templating

H1) Russian Doll Templated Synthesis of *c*-P12



To a solution of **T6•c-P6•(Ar'CO₂)₆** (1.5 mg, 0.23 μmol) in dry CHCl₃ (830 μL, 0.28 mM) were added ligand **L1** (0.43 mg, 1.4 μmol, 6.0 equiv, from a 0.19 M solution in MeOH) and **I-P4** (3.0 mg, 0.7 μmol, 3.0 equiv). After 1 h of stirring at room temperature, the catalyst mixture was added (Pd(PPh₃)₂Cl₂ (0.25 mg, 0.35 μmol, 1.5 equiv), CuI (0.33 mg, 1.8 μmol, 7.5 equiv), 1,4-benzoquinone (0.38 mg, 3.5 μmol, 15 equiv) in dry CHCl₃ (0.21 mL) and dry DIPA (8.5 μL)) and the reaction progress was monitored by UV-vis-NIR spectroscopy. After stirring for 2.5 h, no more spectroscopic changes were observed, after which half a portion of the above described catalyst mixture was added. After stirring for 1 h, the reaction mixture was dried under a stream of N₂ and passed over a short plug of alumina using CHCl₃. The mixture was concentrated under reduced pressure and purified by size exclusion chromatography on Biobeads SX-1 using CHCl₃/10% pyridine to separate the Zn-porphyrin material from the **T6•c-P6•(Ar'CO₂)₆**. Three of these SEC columns were required to separate all Zn-porphyrin material from **T6•c-P6•(Ar'CO₂)₆**. Separation of the Zn-porphyrin products by recycling GPC (toluene/1% pyridine) yielded *c*-P12 (12%, GPC yield) and *c*-P24 (2.5%, GPC yield) as brown solids.

c-P12

¹H NMR (400 MHz, CDCl₃/1% *ds*-pyridine, 298 K): δ_H 9.82 (d, *J* = 4.5 Hz, 24H, β-*H*), 9.03 (d, *J* = 4.5 Hz, 24H, β-*H*), 7.37 (d, *J* = 1.7 Hz, 48H, Ar-*H*_{ortho}), 6.90 (t, 24H, Ar-*H*_{para}), 4.16 (t, 96 H, -OCH₂-), 1.93–1.83 (m, 96H, -CH₂-), 1.57–1.46 (m, 96H, -CH₂-), 1.42–1.20 (m, 384H, -CH₂-), 0.84 (t, *J* = 6.8 Hz, 144H, -CH₃).

***m/z* (MALDI-TOF)** 13004 (C₈₁₆H₉₈₄N₄₈O₄₈Zn₁₂, M⁺ requires 13018).

These data match previous literature reports.^{S5}

c-P24

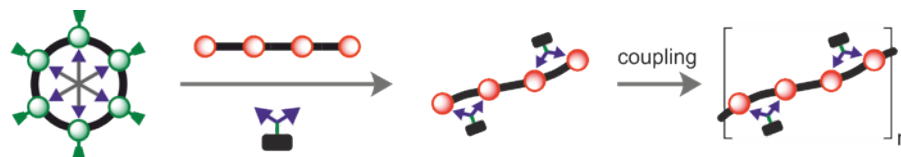
¹H NMR (400 MHz, CDCl₃/1% *ds*-pyridine, 298 K): δ_H 9.88 (d, *J* = 4.5 Hz, 96H, β-*H*), 9.07 (d, *J* = 4.2 Hz, 96H, β-*H*), 7.41 (m, 96H, Ar-*H*_{ortho}), 6.93 (m, 48H, Ar-*H*_{para}), 4.19 (s br, 192, -OCH₂-), 1.95–1.87 (m, 192H, -CH₂-), 1.59–1.50 (m, 192H, -CH₂-), 1.44–1.18 (m, 768H, -CH₂-), 0.91–0.78 (m, 288H, -CH₃)

***m/z* (MALDI-TOF)** 26170 (C₁₆₃₂H₁₉₆₈N₉₆O₉₆Zn₂₄, M⁺ requires 26035).

These data match previous literature reports.^{S12,S13}

Note: The aryl solubilizing side-group on the linear tetramer **I-P4** used in these reactions was 3,5-bis(octyloxy)phenyl.

H2) Control Reaction



To a solution of **T6•c-P6•(Ar'CO₂)₆** (1.5 mg, 0.23 μ mol) in dry CHCl₃ (830 μ L, 0.28 mM) were added protected ligand **Bn-L1** (0.56 mg, 1.4 μ mol, 6.0 equiv, from a 0.16 M solution in MeOH) and **I-P4** (3.0 mg, 0.7 μ mol, 3.0 equiv). After 1 h of stirring, catalyst mixture was added (Pd(PPh₃)₂Cl₂ (0.25 mg, 0.35 μ mol, 1.5 equiv), CuI (0.33 mg, 1.7 μ mol, 7.5 equiv), 1,4-benzoquinone (0.38 mg, 3.5 μ mol, 15 equiv) in dry CHCl₃ (0.21 mL) and dry DIPA (8.5 μ L)) and the reaction progress was monitored by UV-Vis spectroscopy. After stirring for 2.5 h, half a portion of the above described catalyst mixture was added. After stirring for 1 h, the reaction was dried under a stream of N₂ and passed over a short plug of alumina using CHCl₃. The majority of **I-P4** starting material had polymerized. Therefore after the alumina plug only very little material was left. The resulting mixture was concentrated under reduced pressure and purified by size exclusion chromatography (SEC) on Biobeads SX-1 using CHCl₃/10% pyridine to separate the Zn-porphyrin material from the **T6•c-P6•(Ar'CO₂)₆**. An additional SEC column was required to separate all Zn-porphyrin material from **T6•c-P6•(Ar'CO₂)₆**. The Zn-porphyrin fraction was concentrated under reduced pressure and analyzed by analytical recycling GPC (toluene/1%pyridine). The resulting GPC trace is depicted in section *H4*.

Note: The aryl solubilizing side-group on the linear tetramer **I-P4** used in these reactions was 3,5-bis(octyloxy)phenyl.

H3) UV-Vis-NIR Spectra

A strong change in UV-vis-NIR absorption spectrum was observed for the Russian doll templated synthesis of **c-P12** upon reaction completion. The appearance of the distinct band at 869 nm is indicative of porphyrin oligomer formation (including **c-P12**) and marked the completion of the reaction. After the alumina plug – during which the longer insoluble polymeric materials are removed – the absorption pattern from **T6•c-P6** as well as from the porphyrin oligomers are clearly visible. In contrast, at the end of the control reaction, the band originating from porphyrin oligomers is less sharp in the UV-vis-NIR spectrum. The control reaction contained a substantial amount of insoluble material which is reflected in the UV-vis-NIR spectrum after the alumina plug, which shows that there is hardly any porphyrin oligomer material left but mainly **T6•c-P6•(Ar'CO₂)₆** which is seen by the characteristic three peaks at 822, 785 and 752 nm.

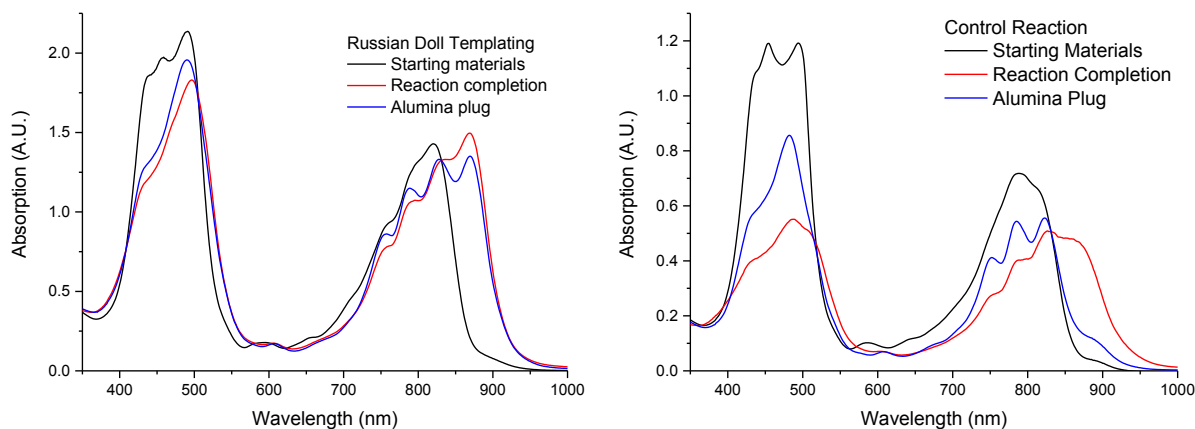


Figure S44. UV-vis-NIR spectra of the Russian doll templating reaction (left) and the control reaction (right). Absorption spectra of: starting materials after stirring for 1 h (black traces), after reaction completion (red traces) and after the alumina plug (blue traces). All spectra were recorded in CHCl₃ and normalized (at 831 nm).

H4) Analytical GPC Traces

The analysis of the product mixtures of the Russian doll templating reaction and the control reaction was performed by gel permeation chromatography (GPC). It has been previously shown that GPC is a powerful tool for separating and at the same time characterizing large porphyrin nanostructures.^{S14}

To be able to compare relative yields, for both reactions all obtained Zn-porphyrin material was injected. In Figure S45 the GPC traces of both reactions are depicted at their absolute scale (i.e. both have the same range on the y-axis). From this representation it is evident how little material was obtained from the control reaction since most material was lost as insoluble polymer.

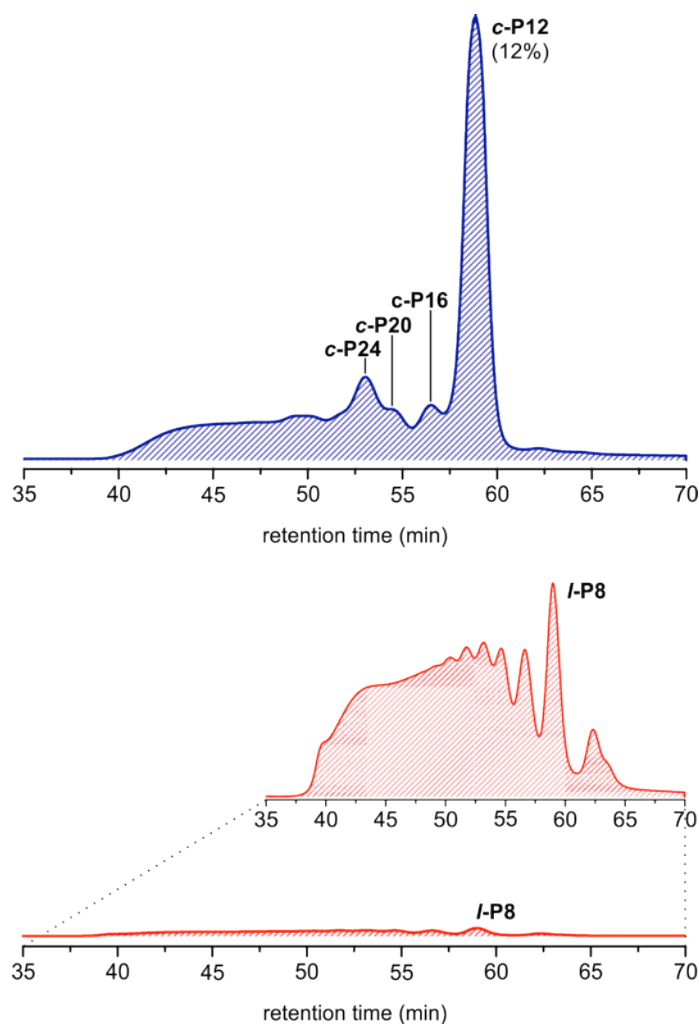


Figure S45. GPC traces (toluene/1% pyridine) of the Russian doll templated synthesis of *c*-P12 (top trace) and the corresponding control reaction (red trace). The identity of the products was determined by calibrated retention times, MALDI-TOF analysis and ¹H-NMR spectroscopy for *c*-P12 and *c*-P24.

H. References

- S1 Jerschow, A.; Müller, N. *J. Magn. Reson.* **1997**, *125*, 372.
- S2 Taylor, P. N.; Anderson, H. L. *J. Am. Chem. Soc.* **1999**, *121*, 11538.
- S3 Hoffmann, M.; Kärnbratt, J.; Chang, M.-H.; Herz, L. M.; Albinsson, B.; Anderson, H. L. *Angew. Chem. Int. Ed.* **2008**, *47*, 4993.
- S4 Sprafke, J. K.; Kondratuk, D. V.; Wykes, M.; Thompson, A. L.; Hoffmann, M.; Drevinskas, R.; Chen, W.-H.; Yong, C. K.; Kärnbratt, J.; Bullock, J. E.; Malfois, M.; Wasielewski, M. R.; Albinsson, B.; Herz, L. M.; Zigmantas, D.; Beljonne, D.; Anderson, H. L. *J. Am. Chem. Soc.* **2011**, *133*, 17262.
- S5 O'Sullivan, M. C.; Sprafke, J. K.; Kondratuk, D. V.; Rinfray, C.; Claridge, T. D. W.; Saywell, A.; Blunt, M. O.; O'Shea, J. N.; Beton, P. H.; Malfois, M.; Anderson, H. L. *Nature* **2011**, *469*, 72.
- S6 Kasibhatla, S. R.; Bookser, B. C.; Xiao, W.; Erion, M. D. *J. Med. Chem.* **2001**, *44*, 613.
- S7 Ikeuchi, K.; Ido, S.; Yoshimura, S.; Asakawa, T.; Inai, M.; Hamashima, Y.; Kan, T. *Org. Lett.* **2012**, *14*, 6016.
- S8 Anezaki, S.; Yamaguchi, Y.; Asami, M. *Chem. Lett.* **2010**, *39*, 398.
- S9 Davidson, G. J. E.; Tong, L. H.; Raithby, P. R.; Sanders, J. K. M. *Chem. Commun.* **2006**, *29*, 3087.
- S10 Davidson, G. J. E.; Lane, L. A.; Raithby, P. R.; Warren, J. E.; Robinson, C. V.; Sanders, J. K. M. *Inorg. Chem.* **2008**, *47*, 8721.
- S11 Hogben, H. J.; Sprafke, J. K.; Hoffmann, M.; Pawlicki, M.; Anderson, H. L. *J. Am. Chem. Soc.*, **2011**, *133*, 20962.
- S12 Yong, C.-K.; Parkinson, P.; Kondratuk, D. V.; Chen, W.-H.; Stannard, A.; Summerfield, A.; Sprafke, J. K.; O'Sullivan, M. C.; Beton, P. H.; Anderson, H. L.; Herz, L. M. *Chem. Sci.* **2015**, *6*, 181.
- S13 Kondratuk, D. V.; Perdigao, L. M. A.; O'Sullivan, M. C.; Svatek, S.; Smith, G.; O'Shea, J. N.; Beton, P. H.; Anderson, H. L. *Angew. Chem. Int. Ed.* **2012**, *51*, 6696.
- S14 Kondratuk, D. V.; Perdigao, L. A.; Esmail, A. M. S.; O'Shea, J. N.; Beton, P. H.; Anderson, H. L. *Nature Chem.* **2015**, *7*, 317.